

---

## Dissolved Fe and Fe-binding organic ligands in the Mediterranean Sea GEOTRACES G04

Gerringa L. J. A. <sup>1,\*</sup>, Slagter H. A. <sup>1</sup>, Bown Johann <sup>1</sup>, Van Haren H. <sup>1</sup>, Laan P. <sup>1</sup>, De Baar H. J. W. <sup>1</sup>, Rijkenberg M. J. A. <sup>1</sup>

<sup>1</sup> NIOZ Royal Netherlands Institute for Sea Research, Department of Ocean Systems (OCS), Utrecht University, P.O. Box 59, 1790 AB Den Burg, Texel, The Netherlands

\* Corresponding author : L. J. A. Gerringa, email address : [loes.gerringa@nioz.nl](mailto:loes.gerringa@nioz.nl)

---

### Abstract :

Dissolved Fe (DFe) and Fe-binding dissolved organic ligands were analysed during two GEOTRACES cruises in the Mediterranean Sea in May and August 2013.

DFe was relatively high near the surface probably due to atmospheric sources, whereas below 500-700 m depth the concentrations were relatively low, < 0.4 nM, compared to typical concentrations of 0.6 nM at the same depths in the Atlantic Ocean. These relatively low concentrations are probably due to scavenging and ballasting by dust particles settling down through the water column. Especially in the Eastern Basin, and more prominent in its northern part, distinct patches with high DFe, up to 8.40 nM, were found between 200 and 3000 m depth. These patches were local, which indicates a point source and lateral transport from this source. Some of these patches coincided with sloping density lines indicating enforced along-frontal currents providing lateral transport of DFe. Sources are probably seamounts and mud volcanoes, which were found to exist at the same depths as the elevated DFe. It is conceivable that a large eddy keeps infusions of DFe isolated from mixing with other water masses. These infusions could originate from slopes or from downwards cascading materials out of canyons.

Fe-binding dissolved organic ligands increase the solubility of Fe enabling high dissolved Fe concentrations, and hence longer residence time. These ligands had median total concentrations between [Lt] = 0.77 and [Lt] = 1.74 nEq of M Fe and conditional stability constants between  $\log K' = 21.57$  and  $\log K' = 22.13$  (N = 156). Median values of [Lt] were higher in the upper 100 m and its median concentration increased from west to east. The [Lt] concentrations did not relate to water mass or DFe concentration. The ligands were nearly saturated with Fe where DFe was elevated near the surface and completely saturated, ratio [Lt]/DFe 1, in patches with high DFe at depth. The high DFe concentrations in these patches are extreme, if not even maximum, concentrations as any surplus Fe with respect to the ligands will tend to precipitate. Calculated inorganic Fe concentrations in the Mediterranean had minimum concentrations of 0.23 pM and below 100 m depth median concentrations that varied between 0.68 and 1.99 pM only. This suggests that the inorganic Fe concentration is the result of a steady state between binding by organic ligands and scavenging processes. Thus scavenging will not result in lower inorganic Fe concentrations and in this way the dissolved ligand concentration determines the concentration of DFe in the Mediterranean Sea.

---

## Highlights

► In the sea of Marmara, vertical processes determined the DFe concentrations which were elevated well below the strong pycnocline. ► The Mediterranean Sea has high DFe in the upper 100 m due to dissolution from dust and enabled by Fe-binding organic ligands. ► DFe in the deep Mediterranean is relatively low compared to the deep Atlantic Ocean as a result of scavenging by dust. ► DFe in the deep Mediterranean is high in distinct patches due to a combination of physical processes and specific sources. ► Competition between the dissolved organic ligands and scavenging dust particles determine  $[Fe^*]$  in deep Mediterranean.

**Keywords** : GEOTRACES, Dissolved Fe, Organic ligands, Mediterranean Sea, Dust, Fe speciation

## 1. Introduction

The Mediterranean Sea is surrounded by land and this has a strong influence on the chemical composition of the water and mixing processes therein. It has a surface area of about 2.5 million km<sup>2</sup> and a mean depth of 1500 m, with typical basin depths of 3000 m, while maximum depths exceed 5000 m in its Eastern Basin. In the west, the Mediterranean is connected with the Atlantic Ocean by the Strait of Gibraltar which is 14.3 km wide and has a sill depth of 280 m. The Western and Eastern Basins are divided by the Sicily Strait, with a sill depth of 316 m. In that region and further into the Eastern Basin, volcanic and hydrothermal activities are abundant. In the east, the Mediterranean is connected with the Black Sea via the Sea of Marmara, (average depth 490 m) and the Channel of the Bosphorus (31 km long, 3 km wide, and an average midstream depth of 64 m). These narrow and shallow connections with the Atlantic Ocean and the Black Sea, in combination with high net evaporation, result in the high salinity in the Mediterranean,  $38 < S < 39$ . The Eastern Basin is warmest and most saline.

63 Near-surface, upper 300 m circulation of relatively fresh Atlantic Water is counter-  
64 clockwise (cyclonic) (e.g., Millot, 1999; Millot and Taupier-Letage, 2005). This basin-scale  
65 circulation along the continents is unstable, resulting in smaller, 100 km diameter spin-off  
66 meso-scale eddies. These eddies are mostly found in the southern part of the basins. They are  
67 most intense in the upper 200 m with horizontal speeds up to  $1 \text{ m s}^{-1}$ , but can reach the basin  
68 floor where they have horizontal speeds of typically  $0.05 \text{ m s}^{-1}$ . These eddies can quickly  
69 transport dissolved and particulate materials into the deep through vertical speeds of  $0.01 \text{ m s}^{-1}$ ,  
70 being approximately 1000 m per day (van Haren et al., 2006). Another even faster vertical  
71 transport process occurs in the northern part of the Mediterranean, being one of the few  
72 regions outside of the polar oceans where dense water formation occurs (Voorhis and Webb,  
73 1970; Gascard, 1973). Due to cooling and evaporation by continental winds in winter, surface  
74 waters can become denser than underlying waters so that they sink by turbulent, natural  
75 convective mixing in 0.1-1 km wide ‘chimneys’. The chimneys themselves are part of sub-  
76 mesoscale eddies (Testor and Gascard, 2003), which further mix newly formed deep dense  
77 waters with overlying water masses with the aid of the Earth rotation (van Haren and Millot,  
78 2009). In the Mediterranean, this mainly occurs in the northern part of the Western Basin and  
79 in the Adriatic Sea of the Eastern Basin. This process occurs every year reaching depths of  
80 several hundreds of meters, but roughly every 8 years it reaches all the way to the bottom.  
81 More rarely, every few decades, formation of deep dense water occurs in the Aegean Sea  
82 (Roether et al., 2007).

83 The influence of the surrounding continents on the chemistry of the Mediterranean is  
84 relatively large. In this study we focus on dissolved Fe (DFe). Rivers like the Nile and the  
85 Rhone are sources of dissolved and particulate matter. It is assumed that the influence of  
86 rivers as source of metals like Fe to seas and oceans is modest, since flocculation within the  
87 estuarine zone will remove the majority of these metals (Sholkovitz, 1976; 1993; Boyle et al.,  
88 1977; Dai et al., 1995; Paucot and Wollast, 1997; Tachiwaka et al., 2004). However, lateral  
89 transport of DFe is known to reach very large distances of 1000 km or more in the upper 200  
90 m (De Jong et al, 2012; Rijkenberg et al., 2012) and in the deep ocean (Fitzsimmons et al,  
91 2014). Moreover, nepheloid layers originating from shelves can occasionally cascade down  
92 canyons and cover the whole bottom of the Western Basin (Puig et al., 2013) and groundwater  
93 discharge is important for nutrients in the oligotrophic Mediterranean (Rodellas et al., 2015;  
94 Trezzi et al., 2016). In this way, transport of fluvial materials including Fe and organic matter  
95 reach much further, here bottom nepheloid layers can generate DFe inputs from below.

96 Dust from the Sahara is expected to be a major source of DFe from above (Guieu et al.,  
97 1991; Guieu et al., 1997, 2010b; Spokes and Jickels, 1996; Wagener et al. 2008, 2010) as it is  
98 for Al (Rolison et al., 2015). By using Al as crustal marker Bonnet and Guieu (2006)  
99 concluded that Saharan dust is the main source for atmospheric input of DFe in the North  
100 Western Mediterranean, but according to Heimbürger et al. (2014) dust coming from the  
101 north, i.e. Europe, can also be considerable here. Although mostly considered as a source of  
102 Fe, dust can act as a sink by scavenging and/or ballasting effects (Wagener et al, 2010).  
103 Another major source for DFe might be hydrothermal activity (Lupton et al. 2011; Nomikou  
104 et al., 2013). Two volcanic systems exist in the Mediterranean, the submarine Aeolian Arc  
105 near Sicily and the Aeolian Islands and the Aegean volcanic arc around the island of Santorini  
106 (Lupton et al. 2011; Nomikou et al., 2013).

107 The chemistry of DFe and notably the organic complexation of DFe is essential to keep Fe  
108 that is supplied from internal cycling, as well as from external sources, in solution by  
109 enhancing its solubility and hence increasing its residence time. The concentrations of these  
110 ligands are determining how far DFe can be transported from its fluvial (Powell and Wilson-  
111 Finelli, 2003; Buck et al., 2007; Gerringa et al., 2007; Abualhaija et al., 2015; Mahmood et

112 al., 2015; Bundy et al., 2015), hydrothermal (Bennett et al., 2008; Sander and Koschinsky  
113 2011; Hawkes et al., 2013; Kleint et al., 2016) and atmospheric (Wagener, et al., 2008;  
114 Rijkenberg et al., 2008) sources. Although the Fe-binding dissolved organic ligands are  
115 important, they are poorly defined and little is known about their sources and sinks  
116 (Hopkinson and Barbeau, 2007; Rijkenberg et al., 2008; Boyd et al., 2010; Gledhill and Buck,  
117 2012). Iron-binding organic ligands are ubiquitous in the oceans and in general are more  
118 saturated with Fe in deeper waters than in surface waters. In surface waters DFe is taken up  
119 by phytoplankton, probably ligands are produced by bacteria and possibly phytoplankton,  
120 together creating a high excess ligand concentration over DFe (Gledhill et al. 2004; Gobler et  
121 al., 2004; Butler et al., 2005; Buck et al. 2010; Thuróczy et al., 2010; Poorvin et al., 2011;  
122 Gledhill and Buck, 2012; King et al. 2012; Bundy et al. 2016). Therefore, a high binding  
123 potential exists for Fe released either by mineralisation of organic material or from external  
124 Fe sources via lateral or horizontal transport.

125 There are only a few studies reporting research on Fe-binding dissolved organic ligands  
126 in the Mediterranean (van den Berg, 1995; Wagener et al., 2008). Van den Berg (1995) was  
127 one of the first to measure the Fe-binding ligands in the Western Mediterranean and  
128 concluded that 99% of DFe was organically complexed. He also found that the highest  
129 concentrations of Fe-binding organic ligands occurred in and just below the zone of maximum  
130 fluorescence, indicating an origin from phytoplankton and/or bacteria. Wagener et al. (2008)  
131 investigated the role of dissolved organic ligands in the dissolution of Fe from dust. The  
132 dissolution rate was linearly related to the concentration of Fe-binding dissolved organic  
133 ligands and to dissolved organic carbon (DOC). It is possible that dust is a source of ligands  
134 too (Saydam, and Senyuva, 2002; Gerringa et al., 2006) or triggers bacterial growth and the  
135 production of ligands (Wagener et al., 2008). In this research, DFe and Fe-binding dissolved  
136 organic ligands are studied in the Dutch GEOTRACES Section GA04.

137  
138

## 139 **2 Methods and equipment**

### 140 *Sampling*

141

142 GEOTRACES section GA04 in the Mediterranean consisted of two legs both on board  
143 the Dutch R/V *Pelagia*. A southern cruise (S), 64PE370, started 14 May 2013 departing from  
144 Lisbon (Portugal) and ended in Istanbul (Turkey) on 05 June 2013. A northern cruise (N),  
145 64PE374, left Istanbul on 25 July 2013 and ended in Lisbon on 11 August 2013. Figure 1  
146 shows the cruise tracks and sampling stations.

147 During the southern cruise, 35 S stations were sampled for DFe including 10 stations  
148 sampled for Fe-binding dissolved organic ligands. Stations 1S-4S were in the Atlantic Ocean,  
149 of which station 1S was sampled for Fe-binding dissolved organic ligands. Stations 5S-33S  
150 were sampled in the Mediterranean Sea (station 25 was not sampled). Of these stations 5S,  
151 8S, 11S, 15S, 18S, 21S, 24S and 29S were sampled for Fe-binding dissolved organic ligands.  
152 Stations 34S-36S were sampled in the Sea of Marmara. Here station 36S was sampled for Fe-  
153 binding dissolved organic ligands. During the northern cruise, stations 1N-19N were sampled  
154 for DFe, except for station 16N. Stations 8N, 13N and 17N were sampled for Fe-binding  
155 dissolved organic ligands.

156 The CTD-package consisted of a SeaBird SBE9*plus* underwater unit, an SBE11*plus*V2 deck  
157 unit, an SBE3*plus* temperature sensor, an SBE4 conductivity sensor, a Wetlabs C-Star  
158 transmissiometer (25 cm, deep, red) and an SBE43 dissolved oxygen sensor. The sensors  
159 were freshly calibrated by Seabird. In situ calibrations of the CTD-thermometers (type SBE-3)

160 were done with a Seabird reference-thermometer (type SBE35). For the calibration of the conductivity  
161 sensor, salinity-samples were tapped on board for analysis back home. Most of the casts were tapped  
162 for Winkler titrations in order to calibrate the dissolved oxygen sensor. The Absolute Salinity (SA  
163 in  $\text{g kg}^{-1}$ ) and Conservative Temperature (CT in  $^{\circ}\text{C}$ ) have been computed using the GSW-  
164 software of TEOS-10 (IOC, SCOR, IAPSO, 2010). Density was expressed as sigma-theta, the  
165 density anomaly referenced to the surface Fluorescence was measured as the beam attenuation  
166 coefficient at 660 nm using a Chelsea Aquatracka MKIII fluorometer. The fluorometer signal  
167 was calibrated against Chlorophyll *a* and is expressed as  $\mu\text{g Chl}a \text{ dm}^{-3}$ .

168 Water samples were taken from the ultra-clean NIOZ CTD-frame and filtered over a 0.2  
169  $\mu\text{m}$  filter using  $\text{N}_2$  overpressure in a clean-air laboratory unit (Rijkenberg et al., 2015).  
170 Samples for DFe analysis were acidified immediately after filtration (see below).  
171 Approximately 900 mL samples were taken for the analysis of Fe-binding dissolved organic  
172 ligands. During the southern cruise these samples were stored at  $-18^{\circ}\text{C}$ . Part of these were  
173 analysed on board during the northern cruise, remaining samples were analysed at the NIOZ  
174 home laboratory. Samples taken during the northern cruise were kept at  $4^{\circ}\text{C}$  in the dark and  
175 analysed on board within two days after sampling.

176 Figures of maps and transects were made using ODV (Schlitzer, 2016).

177

178 *Analysis of the characteristics of the Fe-binding dissolved organic ligands*

179

180 Competing ligand exchange adsorptive cathodic stripping voltammetry (CLE-aCSV)  
181 was performed using two systems consisting of a  $\mu\text{Autolab}$  potentiationstat (Metrohm Autolab  
182 B.V.), a 663 VA stand with a Hg drop electrode (Metrohm) and a 778 sample processor with  
183 ancillary pumps and dosimats (Metrohm), all controlled using a consumer laptop running  
184 Nova 1.9 (Metrohm Autolab B.V.). For the on board measurements the VA stands were  
185 mounted on elastic-suspended plywood platforms in aluminium frames developed at the  
186 NIOZ to minimize motion-induced noise. Electrical noise reduction and backup power was  
187 provided by Fortress 750 UPS systems for spike suppression and line noise filtering (Best  
188 Power). Sample manipulations were performed inside class 100 laminar flow hoods  
189 (Interflow B.V., the Netherlands).

190 The characteristics of Fe-binding dissolved organic ligands, that is both the ligand  
191 concentration  $[\text{L}_t]$  (in nano-equivalents of molar Fe, nEq of M Fe) and the conditional binding  
192 constant  $K'$  ( $\text{M}^{-1}$ ) with respect to  $[\text{Fe}^{3+}]$ , commonly expressed as  $\log K'$  are determined using  
193 2-(2-Thiazolylazo)-p-cresol (TAC) as an added measuring ligand (Croot and Johansson,  
194 2000). TAC was used with a final concentration of  $10 \mu\text{M}$ , and the complex  $(\text{TAC})_2\text{-Fe}$  was  
195 measured after equilibration ( $> 6$  hrs). The increments of Fe concentrations used in the  
196 titration were 0 (2x), 0.2, 0.4, 0.6, 0.8, 1.0, 1.2, 1.5, 2, 2.5, 3, 4, 6, and 8 (2x) nM. Using a  
197 non-linear regression of the Langmuir isotherm, the electrical signal recorded in nA (nano-  
198 Ampere) was converted into a concentration in nM, and the ligand concentration  $[\text{L}_t]$  and the  
199 binding strength  $K'$  were estimated (Gerringa et al., 2014).

200 Using  $[\text{L}_t]$  and  $K'$ , the concentration of Fe bound to a natural Fe-binding ligand  $[\text{FeL}]$ ,  
201 the concentration of inorganic Fe  $[\text{Fe}']$  and the concentration of natural unbound ligand  $[\text{L}']$   
202 were calculated under the assumption of chemical equilibrium using:

203 
$$\text{DFe} = [\text{Fe}^{3+}] (1 + 10^{10} + K' [\text{L}'])$$
 Equation 1

204 and the ligand mass balance:

205  $[L_t]=[FeL]+ [L']$ , Equation 2

206 respectively, by repeated calculations using Newton's algorithm (Press et al., 1986).  
207 The parameters from Liu and Millero (2002) were used and from these an inorganic side  
208 reaction coefficient of  $10^{10}$  was obtained, as also determined by Hudson et al. (1992). Only  
209 during the northern cruise separate samples for determination of DFe (see below) were taken  
210 from the un-acidified Fe-binding dissolved organic ligand samples just before the analysis of  
211 the characteristics of the organic ligands. To be able to compare the results from both cruises,  
212 the DFe concentrations from immediately acidified samples were used for the calculation of  
213 the ligand characteristics. In 6 samples this DFe was either missing (4 samples) or so high that  
214 contamination was probable (2 samples). The sample taken at 501 m at station 1S was not  
215 analysed with FIA, DFe from measurements with inductively coupled plasma mass  
216 spectrometry (ICP-MS) was used instead giving comparable results (Middag et al., 2015). The  
217 other missing samples were from station 8N at 260 m, station 13N at 1000 and 1500 m, the  
218 contaminated samples were from station 13N at 100 and 2000 m depth. For these samples  
219 DFe was used which was measured in subsamples taken from the unacidified 1 L bottles just  
220 before analysis of the ligand characteristics and analysed by FIA. Earlier research showed that  
221 DFe in unacidified samples are on average 13% lower due to wall adsorption (Gerringa et al.,  
222 2015). The results of the above mentioned samples do not deviate from the general trend with  
223 depth or between stations and were thus incorporated in the results.

224 The ligand characteristics were calculated with two models, one assuming the presence  
225 of one ligand class and the other assuming the presence of two ligand classes (Gerringa et al.,  
226 2014) (Supplementary Table 1). We were unable to calculate the ligand characteristics for 2  
227 ligand classes because either only one ligand group was present, or ligand characteristics of  
228 the different ligand groups did not differ enough from each other to be distinguished as  
229 separate classes.

230 The side reaction coefficient  $\alpha_{FeL}$  of the organic ligands was calculated as the product of  
231  $K'$  and  $[L']$ ,

232  $\alpha_{FeL}= K' * [L'] = [FeL]/[Fe']$ , Equation 3

233  $\alpha_{FeL}$  reflects the complexation capacity of the dissolved organic ligands to bind with Fe,  
234 which can be seen as its ability to compete for Fe with other ligands and with adsorption sites  
235 on particles. The parameter  $\alpha_{FeL}$  is more robust to characterize the Fe-binding dissolved  
236 organic ligands than the  $K'$  and  $[L']$  separately because the Langmuir equation does not treat  
237  $K'$  and  $[L']$  independently from each other. If an analytical error forces an underestimation of  
238 one, the other is automatically overestimated (Hudson et al., 2003). Moreover, in our  
239 equations,  $[L']$  is, in contrast to  $[L_t]$ , independent of DFe (Thuróczy et al., 2010). The ratio  
240  $[L_t]/DFe$  (Supplementary Table 1) indicates the saturation of the ligands, which are saturated  
241 with Fe if the ratio  $\leq 1$ , and unsaturated when  $> 1$  (Thuróczy et al, 2010).

#### 242 *Flow Injection Analysis of DFe*

243 The DFe concentrations were measured in filtered (0.2  $\mu$ m, Sartorius Sartobran 300)  
244 and acidified (pH 1.8, 2 ml/L 12M Baseline grade Seastar HCl) samples at sea using an  
245 automated Flow Injection Analysis (FIA) (Klunder et al., 2011) and described in detail by  
246 Rijkenberg et al., 2014 Samples were analysed in triplicate and average DFe concentrations  
247 and standard deviation are given in the available in the GEOTRACES GA04 database  
248 (<http://www.bodc.ac.uk>). The data is publicly available in August 2017 when the  
249 GEOTRACES Intermediate Data Product 2016 will be published. On average, the standard  
250 deviation of the measurements was 3.2%, generally being  $< 5\%$  in samples with DFe

251 concentrations higher than 0.1 nM. Only standard deviation (SD) of measurements near the  
252 detection limit of the system were relatively high. The average blank was determined to be at  
253 0.033 nM during the southern cruise and 0.017 nM during the northern cruise. The blank was  
254 defined by the intercept of a low Fe sample loaded for 5, 10 and 20 seconds and was  
255 measured daily. The limit of detection, 0.019 nM during the southern cruise and 0.004 nM  
256 during the northern cruise, was defined as three times the SD of the mean of the daily  
257 measured blanks, loaded for 10 s. To better understand the day-to-day variations, a duplicate  
258 sample was measured again at least 24 hours after the first measurement. The relative  
259 differences between these measurements were of the order of 1-20%, while the largest  
260 differences were measured in samples with low DFe concentrations. To correct for this day-  
261 to-day variation, a lab standard, a sample acidified for more than 6 months, was measured  
262 daily. The consistency of the FIA system over the course of a day was verified using a drift  
263 standard. For the long-term consistency and absolute accuracy, certified SAFe and  
264 GEOTRACES reference material (Johnson et al., 2007) were measured on a regular basis  
265 (Table 1). We did not measure a consistent DFe in the GS reference samples, like we did in  
266 the other references. We do not know the cause, we might have had a contamination in two  
267 GS bottles. The DFe data have been accepted for the GEOTRACES intermediate data product  
268 2017.

### 269 **3 Hydrography**

270 Stations 1S-4S were sampled in the Atlantic Ocean before entering the Mediterranean  
271 Sea. The Mediterranean Outflow Water (MOW) is readily recognized between 500 and 1500  
272 m by higher salinity ( $>36$ ) and lower oxygen concentrations ( $<200 \mu\text{g kg}^{-1}$ ) (Figures 2 A, D).

273 In the Mediterranean, the Atlantic Water (AW) characterized by relatively low salinity  
274 is present in the surface waters ( $<200$  m) of especially the Western Basin. AW streams  
275 counter clockwise through the basins (e.g., Millot, 1999) and becomes warmer and more  
276 saline along its course. Formed in dense water formation areas in the Eastern Basin, the  
277 Levantine Intermediate Water (LIW) between 200 and 600 m in the southern cruise transect  
278 and 100-800 m in the northern cruise transect, streams to the west and spills into the Western  
279 Basin (see also Rolison et al., 2015). It is discernible by its relatively high salinity ( $>38.75$  in  
280 the Eastern Basin and  $>38.5$  in the Western Basin in the southern transect;  $>38.8$  in the  
281 northern transect) and in the northern transect also by its relatively high temperature ( $>14$ -  
282  $14.5^\circ\text{C}$ ) and in the Western Basin by low oxygen (Figures 2 A, B, D, 3 A, B, D). Below LIW,  
283 three deep water masses are distinguished, the Western Mediterranean Deep Water  
284 (WMDW), the Adriatic Mediterranean Deep Water (AdMDW) and the Aegean Mediterranean  
285 Deep Water (AeMDW). The AdMDW is less saline than the AeMDW (Figure 3 A).

286 Water masses are not only separated vertically, but also horizontally, due to their  
287 different formation areas. Horizontally, water masses are separated by fronts, as can be seen  
288 between AdMDW and AeMDW, for example in Figure 3C. Fronts occur around eddies (for  
289 example near stations 7N, 8N and 9N in Figure 3C, as further discussed in section 5.2 in *Deep*  
290 *high DFe patches*), and near continental boundaries. Dynamically, horizontal transitions in  
291 density give rise to along-frontal currents, due to the rotation of the Earth, causing advective  
292 transport. Near continental boundaries and around eddies such currents are expected to be  
293 strongest with velocities ranging between 0.1 and  $1 \text{ m s}^{-1}$  (Millot and Taupier-Letage, 2005).  
294 They become reinforced after dense water formation events, whereby density contrasts are  
295 sharpened. This gives rise to larger along-frontal currents, following vertical convection  
296 events.

297 The Sea of Marmara has a surface layer of about 20 m with a relatively low salinity  
298 influenced by exchange with the Black Sea ( $S = 21.6$  in the east,  $S = 23$  in the west)



299 (Beşiktepe et al., 1994). This layer contains high oxygen concentrations of 213-280  $\mu\text{g kg}^{-1}$   
300 and fluorescence is relatively high, 0.5-1.1  $\mu\text{g dm}^{-3}$  (Figure 4 A, C, E). Below a very steep  
301 pycnocline at 20 to 50 m the salinity is  $>38.7$  and the oxygen is reduced to 10.4-18.4  $\mu\text{g kg}^{-1}$   
302 in the east and to 20-50  $\mu\text{g kg}^{-1}$  in the west. The surface waters are transitional in character  
303 with a short residence time of months (Ünlüata et al., 1990; Beşiktepe, et al., 1994; Rank et  
304 al., 1999). Below 50 m salinity, temperature and oxygen concentrations are nearly  
305 homogeneous. According to Rank et al. (1999) the sub-halocline water is. This uniform deep  
306 water has a residence time of 6 years, which is influenced by intrusions from the  
307 Mediterranean (Rank et al., 1999, Ünlüata et al., 1990).

308

309

#### 4 Results

310 In the following paragraphs, median values are presented per depth layer (0-100m to show  
311 the influences of dust deposition, 100-1000 m to show properties in the LIW, and 1000-  
312 2000m and  $>2000\text{m}$  for properties of the deep water and the deepest basins, respectively) and  
313 per geographical region, the Atlantic Ocean, the Mediterranean Sea, divided in the Western  
314 Basin and the Eastern Basin, and the Sea of Marmara. Medians with interquartile ranges  
315 (IQR) were calculated instead of average because DFe and also [Lt] had maxima in deep  
316 patches, which influenced the average values and increased the standard deviations, making  
317 median values more suitable. Note that for both the Atlantic Ocean and the Sea of Marmara  
318 only one station was sampled for the Fe-binding organic ligand characteristics, and thus the  
319 number of samples (N) is rather low.

320 In the Atlantic Ocean DFe was low in the surface waters (stations 1S-4S) and ranged  
321 from 0.01 to 0.18 nM in the upper 100 m (Figure 5A). The DFe increased with depth to 0.69  
322 nM at 1000 m in the MOW, and slightly decreased to 0.50 nM at depths larger than 3000 m at  
323 stations 1S and 2S (Figure 6A). Closer to the Mediterranean, DFe increased to 0.71-0.99 nM  
324 around 900 m (stations 3S and 4S), also in the MOW, being well below the Camarinal sill  
325 separating the Mediterranean from the Atlantic Ocean (Figures 5A, 6A).

326 In the Mediterranean, the typical vertical profile of DFe was different from those in the  
327 Atlantic Ocean (Figures 6A versus 6B and 6C). In the Mediterranean, DFe was high near the  
328 surface (median DFe in upper 100 m=1.4 nM, IQR = 0.96, N = 290, ranging from 0.20 to  
329 15.35 nM), with highest near-surface DFe at stations in the north of the Eastern Basin  
330 (Figures 6B and 6C; station 27S with 15.35 nM and station 7N with 9.36 nM), decreasing to  
331 relatively low concentrations of  $<0.40$  nM below 500-700 m (Table 2A). These deep  
332 concentrations were relatively low compared to concentrations of 0.5 nM at similar depths in  
333 the Atlantic Ocean (Rijkenberg et al., 2014, Hatta et al., 2015). The lowest deep DFe of 0.09  
334 nM in the Mediterranean was from station 18S at 3263 m. However, very high DFe of up to  
335 8.40 nM existed in distinct patches of both transects between 200 and 3000 m (at station 6N at  
336 1250 m; Figure 5B). These patches were mostly found in the Eastern Basin during our  
337 northern transect, (Figure 5B). The patches varied roughly between 230-400 km in width and  
338 between 400 and 1000 m in height.

339 In the Sea of Marmara, DFe was elevated in the upper 100 m as in the Mediterranean  
340 and ranged between 0.94-4.93 nM. DFe decreased to 0.75-0.33 nM between 100 and 1000 m  
341 and increased close to the bottom only at one station (35S) to 1.80 nM at 1110 m (Figure 6D,  
342 Table 2A).

343 In the Atlantic Ocean, [Lt] varied between 0.54 and 2.01 nEq of M DFe (N=13, Figure  
344 7A) and had a median of 1.1 nEq of M DFe in the upper 100 m, 1.3 nEq of M DFe in the  
345 upper 1000 m and 0.8 and 1.0 nEq of M DFe in the 1000-2000 m below 2000 m, respectively  
346 (Table 2B for IQR and N per depth layer). The median  $\log K'$  per depth layer varied between  
347 21.9 and 22.1 (N = 13). No trend with depth existed, but the values showed more variation in  
348 the upper 500 m and in the two samples taken just above the sediment (Supplementary Table

349 1). The [Lt] in the Mediterranean Sea varied between 0.23 and 5.51 nEq of M DFe (Figures  
350 7B and 7C, Supplementary Table 1). LogK' varied between 20.54 and 24.11. Only 17 LogK'  
351 values out of 156 samples were higher than 22.5. These high values coincided with ligands  
352 that were saturated with Fe or nearly saturated as shown by the ratio [Lt]/DFe ranging  
353 between 0.6 and 2 with an average of 1.2. These high logK' values are influenced by the fact  
354 that the ligands were near saturation and therefore had very few data points in the calculation,  
355 probably resulting in a correct [Lt] but not in very reliable K' by lack of degrees of freedom.  
356 This is illustrated by the high standard errors only 5 of the 17 have an upper SE smaller than  
357 0.4 mol<sup>-1</sup>. Thus we assume that actually logK' varied between 20.54 and 22.5, although all  
358 values were used for calculating means and medians in the following text.

359 In the Sea of Marmara, high [Lt] up to 5.12 nEq of M DFe existed in the upper 100 m  
360 where fluorescence was high, in deeper water [Lt] varied between 0.79-2.21 nEq of M DFe;  
361 whereas logK' varied between 21.97 and 20.90 with no apparent relation with depth (Figure  
362 7D, Table 2B).

363 When comparing the three regions, the median DFe per depth layer increased in the  
364 Atlantic Ocean with depth and decreased with depth in the other three basins (Table 2 A). The  
365 median [Lt] per depth interval generally decreased with depth in all regions. However, in the  
366 Western Mediterranean Basin it remained almost constant with depth between 1.51 and 1.74  
367 nEq of M Fe. (Supplementary Table 1 and Table 2B). The median [Lt] was lowest in the  
368 Atlantic Ocean (0.77-1.27 nEq of M Fe) and highest in the Sea of Marmara, ranging from  
369 0.79 to 2.93 nEq of M Fe. The median values of [Lt] in the upper 0-100 m and 100-1000 m  
370 were higher in the Western compared to the Eastern Basin of the Mediterranean (Table 2B).  
371 The median values of logK' decreased slightly from west to east from 21.71-22.04 in the  
372 Atlantic Ocean, 21.55-21.94 in the Western Mediterranean, 21.57-22.13 in the Eastern  
373 Mediterranean to 21.2-21.82 in the Sea of Marmara.

374 In the Atlantic Ocean, logK' was fairly constant through the water column and ranged  
375 between 21.71 and 22.06. In the Mediterranean, both in the Western and Eastern Basins,  
376 logK' decreased with depth, with an exception between 1000 and 2000 m in the Eastern Basin  
377 where a relatively high logK' was found, 22.13 versus 21.87-21.57. In the Sea of Marmara,  
378 log K' varied between 21.20 and 21.82 unrelated with depth. The Log $\alpha_{\text{FeL}}$  did not vary  
379 between the Atlantic Ocean and the Mediterranean Sea but was lower in the Sea of Marmara  
380 (Table 2 B). Log $\alpha_{\text{FeL}}$  decreased with depth in the Atlantic Ocean from 13.07 to 12.52, it  
381 varied little between 12.36 and 12.84 in the Mediterranean Sea and it increased with depth in  
382 the Sea of Marmara from 10.50 to 12.61. The ratio [Lt]/DFe decreased with depth in the  
383 Atlantic Ocean from relatively high 43.4 in the upper 100 m to values round 1 and 2 in deep  
384 waters whereas in the other regions, the ratio increased with depth. In the Mediterranean and  
385 Sea of Marmara this ratio did not vary as much and remained between 0.7 and 4.45. Excess L  
386 decreased with depth in the Atlantic Ocean and increased with depth in the Mediterranean  
387 basins. In the Sea of Marmara excess L and DFe vary, in the surface DFe is relatively high  
388 and excess L is low (0.01-0.22 nEq of M Fe) (Figure 4, Supplementary Table 1 and Tables 2  
389 A, 2 B).

390

## 391 5. Discussion

392 5.1 Sources and sinks of DFe and Fe-binding dissolved organic ligands in the  
393 Atlantic Ocean and the Sea of Marmara

### 394 *Atlantic Ocean*

395 The depth-profiles of DFe at stations 1S-4S were similar to those observed by others in  
396 the Atlantic Ocean, with very low concentrations near the surface due to phytoplankton  
397 uptake and scavenging by dust, although seasonal increases in DFe are reported due to dust

398 input (Sedwick et al., 2005; Thuróczy et al., 2010; Wagener et al., 2010; Rijkenberg et al.,  
399 2012; 2014; Hatta et al., 2015, Sedwick et al., 2015). Calculated  $[Fe^*]$  are very low 0.02-0.07  
400 in pM in the upper 100 m, lowest values obtained in the present research. Phytoplankton  
401 uptake of Fe was probably the reason for these low values. Increasing DFe concentrations  
402 with depth in the upper 500-1000 m (Figures 5A, 6A) are probably due to the release by  
403 degradation of organic matter and the DFe decrease below 1500 m at stations 1S-3S is  
404 probably due to scavenging (Bruland et al., 2014). Below 2000 m, DFe was close to 0.5 nM  
405 as also observed by Sarthou et al. (2007). Closer to the Strait of Gibraltar (Stations 3S and  
406 4S), DFe was higher in the MOW between 500 and 2000 m. Since the salinity and the density  
407 were also higher and the oxygen concentrations were lower at these depths (Fig 2 A,C,D), it is  
408 safe to conclude that the Mediterranean is the source of elevated DFe. Although they expected  
409 elevated DFe, Hatta et al. (2015) did not detect higher DFe in the MOW at their stations, in  
410 the same region as our stations. Also Thuróczy et al. (2010) did not detect elevated DFe in  
411 MOW at the position of our station 1S. However, at depths of the MOW Thuróczy et al.  
412 (2010) measured an increase in particulate Fe (PFe). Lenses of MOW, 'Meddies' or pulses of  
413 water are released into the Atlantic at different depths depending on density. These move with  
414 variable velocities and directions and are also dependent on season. In this way these  
415 hydrological features explain variability in DFe and it is thus not surprising that results are not  
416 overlapping here (Ambar et al., 2008).

417 The calculated values of  $\log\alpha_{FeL}$  for both the present study and that of Thuróczy et al.  
418 (2010) compare well, with values between 12.71 and 13.25 from their study and 12.05 and  
419 13.35 from this study. In both studies ligands got more saturated with depth until 1000-2000  
420 m, below which  $[Lt]/DFe$  remained constant with depth. At our station 1S, excess L and  $[Fe^*]$   
421 also remained constant below 1000 m. Apparently at this depth a steady state is reached for Fe  
422 between binding by organic ligands and scavenging by marine snow (Bruland et al., 2014).  
423 The  $[Lt]$  is slightly higher at 1000 m in the MOW. It is thus possible that the Mediterranean is  
424 also a source of dissolved organic Fe-binding ligands for the Atlantic Ocean. Buck et al.  
425 (2015) measured ligand characteristics East and South of the Strait of Gibraltar. They  
426 distinguished three different ligand groups with a sum  $[Lt]$  around 2-3 nEq of M Fe, higher  
427 than the concentrations at our station 1S. However,  $\log\alpha_{FeL}$  was between 13 and 13.5, which is  
428 close to our values of 12.05 and 13.35. This confirms that the side reaction coefficient ( $\log\alpha$ )  
429 is a useful parameter for comparing results of speciation data obtained with different chemical  
430 and mathematical methods (Town and Filella, 2000; Hudson et al., 2003; Gerringa et al.,  
431 2016; Gledhill and Gerringa, submitted)

432

#### 433 *Sea of Marmara*

434 In the Sea of Marmara the elevated DFe up to 4.93 nM was not restricted to the upper  
435 20-50 m, the layer influenced by the outflow of the Black Sea with low salinity high oxygen  
436 and high fluorescence, but it extended over 100 m. Below 100 m DFe decreased from 1.21 to  
437 0.18 nM. Changes in DFe are not related to changes in oxygen concentration (Figure 4 D,E).  
438 The sources of Fe are predominantly in the surface and determine the depth distribution in the  
439 upper 100 m. The sea is relatively polluted although not in Fe as concluded in sediment  
440 studies (Pekey, 2006). The sea is surrounded by land, with lateral supply from rivers like the  
441 polluted Dil Deresi, and from the Black Sea. The organic ligands at station 36S were weaker  
442 than in the Atlantic Ocean and in the Mediterranean Sea (see below). However, the lower  
443 conditional binding constants had comparable values between 20.74 and 22.2, obtained with  
444 the same method in the near-surface oxic layer of the Black Sea (Gerringa et al., 2016). The  
445 relatively high  $[Lt]$  between 1 and 2.8 nEq of M Fe in the Black Sea also compared rather  
446 well to the values between 0.79 and 5.12 nEq of M Fe in the Sea of Marmara confirming the  
447 role of the Black Sea as a source. Near the surface, the ligands were saturated at station 36S,

448 excess L is very low and the three lowest [Lt]/DFe ratios in this research are found here; thus  
449 DFe concentrations were quite extreme if not maximum concentrations in the upper 100 m.  
450 The 100 m deep layer with elevated DFe can be explained by sinking particles, predominantly  
451 dust, releasing Fe enabled by excess L. Some of the sources for Fe, most probably rivers and  
452 the Black Sea may be important for the dissolved organic Fe-binding ligands as well. The  
453 proximity of land increases the chance that humic substances are an important part of the Fe-  
454 binding ligand pool. This ligand group might be underestimated by our method, which is not  
455 very sensitive for humic substances (Laglera et al, 2011; Abualhaija et al., 2015; Bundy et al.,  
456 2015).

## 458 5.2 Sources and sinks in the Mediterranean

459 As in other seas and oceans DFe and [Lt] do not systematically vary with water masses  
460 (Rijkenberg et al., 2014; Bruland et al., 2014; Gerringa et al., 2015; Buck et al., 2015;  
461 Thuróczy et al, 2011; Klunder et al., 2012). Even the LIW, considered to be an important  
462 water mass in the Mediterranean, cannot be recognized in both transects of DFe (Figures 2A,  
463 3A and 5), as was also concluded by Rolison et al. (2015) for DAl in the southern cruise. This  
464 most likely indicates the strong influence of vertical processes above the effect of horizontal  
465 processes. However in the West Atlantic Ocean, Gerringa et al. (2015) reported that [Lt]  
466 decreased along the flowpath of the NADW.

467

### 468 *Near-surface waters*

469 The high DFe concentration in the upper 100 m of the Mediterranean (Figures 5 A, B,  
470 and 6 B, C) suggests that dust is a major source of DFe, predominantly from the Sahara but  
471 also from anthropogenic sources (Guieu et al., 1991; 1997; 2010a; 2010b; Croot et al., 2004;  
472 Rijkenberg et al., 2008; Aguilar-Islas et al., 2010; Buck et al., 2010; Heimbürger et al., 2014).  
473 Guieu et al. (2010a) concluded that an increase in DFe up to 5.3 nM in the surface mixed  
474 layer in the Western Basin was due to dust input, with smaller concentrations in the Eastern  
475 Basin. In that study, the fluxes of dust and thus metals varied strongly depending to the season  
476 and weather conditions. We found the highest DFe concentrations, close to Greece and in the  
477 Adriatic Sea. Along the southern transect, Rolison et al. (2015) also measured higher surface  
478 dissolved Al (DAl) in the Eastern Basin than in the Western Basin. River input of metals is  
479 expected to be important close to the coasts, although a large fraction of DFe and other  
480 dissolved metals may be lost by flocculation upon mixing with saline waters (Boyle et al,  
481 1977; Sholkovitz, 1976; Paucot and Wollast, 1997; Buck et al., 2007). Lateral transport of the  
482 remaining river DFe enabled by complexation (Jones et al., 2011) is most probably occurring  
483 at such a small scale that it is hard to be distinguished by us since we sampled far from the  
484 coast along the deepest part of the Mediterranean Sea. Except for stations in the Northeast  
485 (stations 26S-33S) and near the Adriatic Sea (stations 7N, 8N, 9N) where the cruise track  
486 came relatively close to the coast and rivers and lateral transport from land could play a role  
487 as source, dust is most probably the main source for the high near-surface DFe at our station  
488 locations in the Mediterranean.

489 The importance of dust as source of DFe depends on the amount of dust, its Fe content  
490 and on the solubility of Fe. Fe-binding organic ligands in aerosols, like oxalate or aliphatic  
491 water soluble organic carbon compounds, increases the solubility of Fe from the dust (Paris et  
492 al., 2011; Wozniak et al., 2015). The solubility in seawater depends also on the nature of the  
493 dust particles (Visser et al., 2003; Baker and Jickells, 2006; Sedwick et al., 2007; Baker and  
494 Croot, 2010; Fishwick et al., 2014). Journet et al. (2008) found that Fe solubility of clays  
495 (illite) was even larger than that of Fe-oxides in dissolution experiments. However, also the

496 characteristics and composition of the seawater influences Fe dissolution. Logically, it can be  
497 deduced that the solubility of Fe from dust is related to the excess ligand concentration in  
498 seawater. Indeed, Rijkenberg et al. (2008) found that the Fe-binding ligands play a key role in  
499 keeping Fe from Sahara dust in solution, as also concluded by Aguilar-Islas et al. (2010) in  
500 the Pacific and Fishwick et al. (2014) in the Sargasso Sea.

501 Wagener et al. (2008) found that the dissolution rates of Fe from Sahara dust were  
502 linearly related to the concentration of dissolved organic ligands in sea water. Interestingly,  
503 they discovered that excess ligands were not always successful in dissolving Fe. The  
504 dissolving capacity depended on the season and probably on the presence of freshly produced  
505 ligands by biota. Our cruises were in summer, with relatively high biological activity (Van der  
506 Poll et al., 2015). Probably the presence of freshly formed ligands enabled a high solubility of  
507 Fe (Barbeau et al., 2001). Wagener et al. (2010) concluded that successive dust depositions  
508 could have different biogeochemical reactions near the surface of the Mediterranean. They  
509 found that repetitive dust depositions in mesocosms studies had opposite effects, no flux of Fe  
510 from the dust into the seawater occurred, the opposite happened, the dust particles cleaned the  
511 water column from Fe and scavenged DFe out of the water. Sarthou and Jeandel (2001)  
512 showed that near the surface in the north of the Western Basin the exchange flux of Fe from  
513 the dissolved to the particulate phase was high, but decreased considerably with depth.  
514 According to Aguilar-Islas et al. (2010) and Fishwick et al. (2014) the dissolved Fe from dust  
515 was predominantly in the colloidal fraction. The distribution over different size fractions of Fe  
516 and the Fe-binding ligands is influencing the dissolution and residence time of Fe. This is  
517 discussed elsewhere and is outside the scope of this study (Wu et al., 2001; Croot et al., 2004;  
518 Fitzsimmons et al., 2015). Thus, DFe is the resultant of dissolution and scavenging and  
519 ballasting effects of Sahara dust. The dissolution of Fe from dust depends, apart from the  
520 nature of the dust, on the nature of the ligands (Wozniak et al., 2015; Aguilar Islas et al.,  
521 2010) and on the age of the ligands (Wagener et al., 2010), as well as on the dust history of  
522 the environment.

523 Even if this is not as apparent as for DFe, [Lt] is also higher near the surface (Figures 7  
524 B, C). Sources for Fe-binding dissolved organic ligands can be biological activity (Barbeau et  
525 al., 2001; Rue and Bruland, 1995; Gerringa et al., 2006; Gledhill et al., 2004) and in the east  
526 the Black Sea as an additional source (Gerringa et al., 2016). Due to the high DFe, the growth  
527 of phytoplankton was not limited by a lack of Fe. According to Van de Poll et al. (2015),  
528 describing the southern transect, phytoplankton was nitrate-limited in the Eastern as well as in  
529 the Western Mediterranean Sea. If there is production of siderophores it is not to relieve Fe  
530 stress, only ligands resulting from degradation and viral lysis should be formed (Poorvin et  
531 al., 2011; Slagter et al., 2016). In the Western Basin diatoms were abundant, in the Eastern  
532 Basin *Synechococcus* was most abundant. In the Western Basin chlorophyll had maximum  
533 concentrations in the upper 50 m, while in the Eastern Basin its maximum was found between  
534 100 and 130 m (Van der Poll et al., 2015). No relationship could be detected between  
535 fluorescence and [Lt] in the southern transect. However, sample depths for DFe and [Lt] were  
536 not concentrated at the near-surface layer, the photic zone, hampering a detailed comparison  
537 of DFe and Lt versus fluorescence.

538 Dust is another potential source of Fe-binding ligands (Johansen et al., 2000; Saydam et  
539 al., 2002; Gerringa et al., 2006; Paris et al., 2011; Wozniak et al., 2015). Although [Lt] was  
540 relatively high in the upper 100 m, the ratio [Lt]/DFe was lowest compared to deeper waters.  
541 The ligands were not completely saturated with Fe, since the ratio was almost never below 1,  
542 as it was the case in the Sea of Marmara. The median [Lt]/DFe was 1.4 in the upper 100 m in  
543 the Western Basin and 1.15 in the Eastern Basin. The median of DFe was 0.34 nM higher in  
544 the Eastern compared to the Western Basin, whereas the median in [Lt] was only slightly, 0.1  
545 nEq of M DFe, higher in the Eastern Basin compared to the Western Basin. Assuming that

546 dust is the source, it is apparently not an equally important source for dissolved organic Fe-  
547 binding ligands as it is for Fe. Dust as a sink for Fe-binding ligands is as far as we know not  
548 considered, yet scavenging and ballasting of organically complexed Fe must take place since  
549 almost all DFe is complexed. We can conclude that the elevated DFe, above its inorganic  
550 solubility, near the surface of the Mediterranean Sea is possible due to the complexation by  
551 dissolved organic ligands.

552

### 553 *Deep waters*

554

555 Apart from distinct patches with elevated concentrations, which are further discussed in the  
556 next section, DFe was relatively low below 300 m along the southern transect and below 500  
557 m along the northern transect. In most samples DFe was lower than in open oceans at similar  
558 depths. Station 18S and station 13N are good examples with deep DFe between 0.09 and 0.30  
559 nM and 0.19 and 0.27 nM, respectively. Surface DFe inputs from Sahara dust did not impact  
560 deep waters which could be due to DFe scavenging by sinking dust itself. Wagener et al.  
561 (2010) showed that Sahara dust supply does not always increase DFe. On the contrary, they  
562 showed that through scavenging DFe can be stripped from the dissolved phase by settling  
563 dust. Due to this scavenging a direct relationship between dissolution and excess ligands is  
564 not always straightforward. It is very probable that settling dust particles scavenge Fe even  
565 though it is in its organically complexed form. Subsequently, due to the decrease of inorganic  
566 Fe (Fe<sup>'</sup>) by scavenging, Fe can dissociate from the ligands, emptying the ligands over time  
567 and depth as shown by an increase in the ratio [Lt]/DFe with depth. Such an increase in the  
568 ratio indeed happened for stations 8S and 18S (Figure 8 B), but not for stations 21S and 24S  
569 which have high DFe patches at 2000 and 1250 m, respectively. Along the northern transect,  
570 an increase in the ratio was observed for stations 13N and 17N, but again not for station 8N,  
571 where high DFe patches existed (Figures 5 B, 8 C). The removal of Fe from the organic  
572 ligand complex has also been suggested by Thuróczy et al. (2011) for the Makarov Basin of  
573 the Arctic Ocean. The Arctic Ocean is far from being a dust impacted area, but due to the very  
574 long residence times of Deep Makarov Basin Water, scavenging was likely the reason for the  
575 decrease in DFe and the simultaneous increases in [L'] and therefore the increase of the  
576 [Lt]/DFe ratio with depth. In the present research the median of calculated concentrations of  
577 [Fe<sup>'</sup>] below 1000 m are close to 1 pM (0.7-1.7 pM). This is comparable to [Fe<sup>'</sup>] at the same  
578 depths for our station 1S in the Atlantic Ocean as well as in the North Western Atlantic Ocean  
579 (median 0.2-0.5 pM from three cruises in the Western Atlantic Ocean, Gerringa et al., 2015;  
580 Table 2B). Because [Fe<sup>'</sup>] is calculated using the ligand characteristics which depend on the  
581 analytical method (Laglera et al., 2011; Buck et al., 2012; 2016; Abualhaija et al., 2015) and  
582 on how the parameters were calculated (Laglera et al., 2013; Gerringa et al., 2014; Pižeta et  
583 al., 2015; Buck et al., 2016) we only compare our data with data collected using the same  
584 methods. The methods in this research were also applied in the Western Atlantic, Gerringa et  
585 al. (2015) concluded that [Fe<sup>'</sup>] between 0.2 and 1 pM represent an equilibrium or steady state  
586 concentration between complexation by organic ligands and scavenging. Only where ligands  
587 were saturated with Fe, near hydrothermal vents where DFe was relatively high, [Fe<sup>'</sup>] were  
588 higher. In the present research median values in the deep (>1000 m) Atlantic Ocean and  
589 Mediterranean Sea vary between 0.52 and 3.44 pM and 0.68 and 1.99 pM, respectively and  
590 are never below 0.23 pM (Supplementary table 1). According to equation 3 the values of  
591  $\log\alpha_{\text{FeL}}$  should show the same small but reversed range by a factor 3 since high  $\alpha$  results in  
592 low [Fe<sup>'</sup>]. Median values of  $\log\alpha_{\text{FeL}}$  (values expressed with respect to Fe<sup>3+</sup>) of 12.49-12.84  
593 existed at depths >100m in Mediterranean waters, slightly higher than in the Western Atlantic  
594 Ocean with  $\log\alpha_{\text{FeL}}=13.1$  (Table 2B, Supplementary Table 1). Both the relatively small  
595 variation in [Fe<sup>'</sup>] and in  $\log\alpha_{\text{FeL}}$  outside the deep high Fe patches indicate an equilibrium or

596 steady state for Fe<sup>2+</sup> that exist between the organic ligands and scavenging particles. At a lower  
597 [Fe<sup>2+</sup>], Fe is so firmly bound that scavenging is hardly possible.

598

#### 599 *Deep high DFe patches*

600 The high DFe patches could be ascribed to Fe supply by (i) lateral transport from land  
601 and shelves, (ii) vertical transport from the sediment and (iii) vertical and lateral transport  
602 from hydrothermal vents. These processes might be reflected by elevated particle densities.  
603 Particle densities can be related to the attenuation coefficient. The attenuation coefficient is  
604 high in the surface probably due to phytoplankton (Figures 2 E, F, 3 E, F). Evidence of  
605 particles elsewhere is scarce. Along the southern transect only near the Straits of Gibraltar and  
606 Sicily, elevated attenuation coefficients coincide with slightly elevated DFe (stations 5S and  
607 6S near 1000m depth and stations 11S and 12S at 2000 and 2500m depth, respectively).

608 Along the northern transect more deep patches with higher DFe were found (Figure 5  
609 B). The attenuation coefficient is slightly higher near the bottom in the Western Basin, at  
610 station 15N, not coinciding with elevated DFe. It is also higher near the sills, especially near  
611 stations 7N, 8N and 9N (no data for station 6N exists) at the entrance of the Adriatic. The  
612 patches of elevated DFe at stations 7N, 8N and 9N are located at the southern end of the  
613 Adriatic Sea. At these stations, especially the most northern station 8N, the attenuation  
614 coefficient and oxygen are also elevated (Figure 3 D, F) and temperature is lower (Figure 3B).  
615 Elevated oxygen, higher than elsewhere in the Mediterranean, occurred also near the bottom  
616 at station 6N in the direction of the Aegean Sea at 1500 m. This is unexpected since the  
617 Adriatic Sea is known to suffer from anoxic periods (Koron et al., 2015). Elevated oxygen  
618 points to recent contact with the atmosphere and thus recently formed deep water. The  
619 attenuation coefficient is high and the temperature (<13.5°C) and salinity are low. Indeed this  
620 cold water can be identified as AdMDW originating from the shallow northern Adriatic where  
621 it formed in winter (Pollak, 1951). The DFe is elevated over almost the whole water column  
622 of stations 7N, 8N and 9N except for the deep samples 100-200 m above the sediment,  
623 apparently AdMDW contains less DFe. The elevated DFe in the layer just above the AdMDW  
624 is advected by strong currents as evidenced by the large horizontal density gradients (Figure  
625 3C). At station 8N, the ligand characteristics were analysed and the ligands were saturated at  
626 160 and 600 m depth. In between these depths and below 600 m the [Lt]/DFe ratio was  
627 between 1.5 and 3.9, thus enabling this high solubility in almost all depths with calculated  
628 [Fe<sup>2+</sup>] between 0.3 and 1 pM. At 160 and 600 m depth, the calculated [Fe<sup>2+</sup>] is 231 and 316 pM  
629 above the solubility of Fe, this DFe is expected to be labile and either complexed to relatively  
630 weak dissolved organic ligands outside the detection window of our method, or present as  
631 inorganic colloids. If we assume that particles above the sediment are the source, dissolved  
632 organic ligands enable Fe to stay in the dissolved phase and explain that DFe diffused away  
633 from the source (Klunder et al. 2012; Thuróczy et al, 2011).

634 Highest deep DFe exists at mid depth, 0.81 nM at station 17N, 3.42 nM at station 18N  
635 and 1.35 nM at station 19N at 1750, 1750 and 1500 m, respectively. Samples from station  
636 17N have been analysed for organic ligands. At 1750 m depth the [Lt]/DFe ratio is 1.5, and  
637 thus ligands were not saturated, enabling the high DFe of 0.81 nM. These three stations are  
638 relatively far from islands and coasts. There is no information about hydrothermal activity  
639 here that could explain this elevated DFe. Density contours below 1000 m bend downward  
640 from stations 17N and 19N to station 18N. This suggests a deep mesoscale eddy, which is the  
641 prominent feature in the mid-southern part of the Western Basin (Millot and Taupier-Letage,  
642 2005; Schroeder et al., 2008). Apparently, DFe is transported by such an eddy. At these  
643 stations the densest water with relatively strong stratification is found below 2400 m, while  
644 the beam attenuation coefficient is only increasing in the lower 150 m above the bottom. Thus

645 there is no indication that enhanced DFe results from deep-water formation. From our results  
646 we cannot distinguish the possible sources of DFe here.

647 The stations 1N-9N, 11N, 12N and 15N are closer to land and thus lateral transport  
648 from shelves and islands can be the source of DFe here. Still more than one specific source of  
649 DFe must exist to explain the multiple deep elevated DFe patches. These are mainly found  
650 between 1000 and 2500 m (Figures 5 B, 6 B, C). The depth differences indicate that not one  
651 source but at least three different sources for the three different depths are involved. From  
652 such sources the enhanced DFe spreads relatively slowly through the basins. The spreading is  
653 partially diffusive, as suggested from the form of the DFe profiles around the depths where  
654 maximum DFe is found, a gradual decrease above and below the maximum DFe. This  
655 diffusive spreading across density stratification is likely dominated by turbulence, enforced by  
656 internal wave breaking, in the vicinity of topography (van Haren et al., 2014). Horizontally,  
657 the spreading is via boundary currents near topography and eddies further in the interior. Such  
658 eddies are observed (Figures 2 C, 3 C) in the upper 500 m nearly everywhere, but especially  
659 strong in the Adriatic Sea. These eddies can explain transport of DFe to the high DFe patches,  
660 at station 6N (1000-1500 m), stations 7N, 8N and 9N (400-800 m) stations 17N-19N (800-  
661 2500 m), and at stations 23S, 24S (1000-1500 m), 27S and 28S (near 700 m). However,  
662 density profiles do not indicate lateral transport for explaining the high DFe patches at station  
663 4N (1500-2200 m), although between stations 4N and 5N there is a horizontal gradient, and  
664 also not at stations 10N-11N (1000-2000 m). In the Southern transect lateral transport is not  
665 supported around station 21S (near 2000 m). Therefore, either the source here is nearby or  
666 transport is in a perpendicular direction to the E-W transect. Horizontal spreading indicates  
667 deep sources, and immediately hydrothermal vents come to mind since they are known deep  
668 sources deemed to be very important (Bennett et al., 2008; Tagliabue et al, 2010; Klunder et  
669 al. 2012; Rijkenberg et al., 2014; Hatta et al., 2015). Although there are two well-known  
670 volcanic active arcs, the Hellenic Arc in the Aegean Sea and the Aeolian Arc in the  
671 Tyrrhenian Sea near Sicily, the thus far known hydrothermal activity is restricted to very  
672 shallow depths of maximum 100 m (Beaulieu et al, 2015).

673 Station 26S, 4100 m deep, is situated at the Rhodes depression which is 4500 m deep,  
674 nearby the Anaximander mountains of approximately 1200 m deep, also known for its mud-  
675 volcanos (Figure 1). Although, as far as we know no references exist indicating mud-volcanos  
676 as a source of DFe, mud-volcanos exist in the Mediterranean Sea at depths that coincide with  
677 the presently observed high DFe patches. For instance the Anaximander Mountains are  
678 associated with faults allowing over-pressured fluids to be erupted at the seafloor and the  
679 Amsterdam mud-volcano (at 35°19.91'N, 30°16.12'E) at 2028 m is the most active (Lazar et  
680 al., 2012). The Texel mud-volcano is located near our station 24S, at 1600 m depth (Zitter,  
681 2004) the Kula and San Remo mud-volcanos are at 1650 m and close to our station 26S. The  
682 Milano mud-volcano is at 1900 m at 34 N, 24.8 E (Bonini and Mazzarini, 2010). The Chefren  
683 mud-volcano at 2900 m (approximately south of station 21S, but not close to this station, at  
684 32.6° N and 28,1° E) has been identified as a potential Fe source as its porewaters have very  
685 high Fe(II) concentrations (up to 1 mM) (Omorigie et al., 2008). Also Southeast of Sicily  
686 near our station 11N mud-volcanos were discovered (Figure 1; Mascle et al., 2014).

687 It is conceivable that deep Fe sources can be formed by nepheloid layers, land, or due to  
688 steep topography and the sides of canyons, while most probably also mud-volcanos play a  
689 role.

690

## 691 **6. Conclusions**

692



693 The Mediterranean Sea and the Sea of Marmara have high DFe in the upper 100 m  
694 probably due to dissolution from dust. In almost all samples [Lt] was larger than DFe thus  
695 enabling the high DFe concentrations.

696 In the Sea of Marmara, vertical processes determined the DFe concentrations which  
697 were elevated not only in the surface 20 m but well below the strong pycnocline (22 to 38 g  
698 kg<sup>-1</sup>).

699 Concentrations of DFe in the deep Mediterranean were either relatively low compared  
700 to the Atlantic Ocean, or relatively high in distinct patches. Deep DFe concentrations in the  
701 Mediterranean Sea were most likely low as a result of scavenging by sinking dust. This  
702 suggestion is the most probable explanation for our results and is supported by results from  
703 mesocosm experiments (Wagener et al., 2010).

704 The presence of distinct patches in deep waters with elevated DFe can only be explained  
705 by a combination of physical processes and sources at specific locations and depths. The  
706 outlines of the deep high DFe patches indicate lateral transport by, for example, mesoscale  
707 eddies from deep sources. These sources are probably diverse, and can be mud-volcanos, land  
708 and deep-sea mountains. Although no previous data is known about mud-volcanos as source  
709 of Fe and no supporting data such as an increase in particle density was observed, mud-  
710 volcanos were located at coinciding depths where high DFe patches were found. In most cases  
711 in these patches the [Lt] was higher than DFe, explaining that these high dissolved  
712 concentrations can exist and be maintained for longer time.

713 Calculated [Fe<sup>3+</sup>] in deep waters were not below 0.23 pM. Apparently this is a steady  
714 state concentration due to competition between the Fe-binding dissolved organic ligands and  
715 scavenging particles. Lower [Fe<sup>3+</sup>] does exist but only in the top 100 m in the Atlantic Ocean,  
716 at our station 1S, indicating that a phytoplankton bloom can lead to lower [Fe<sup>3+</sup>].

717

## 718 Acknowledgements

719 We thank Captain Pieter Kuijt and his crew of *RV Pelagia* for their hospitality and help  
720 during both cruises. The post-cruise data management by Hendrik van Aken and the data  
721 management group was excellent as usual. We thank NIOZ Marine Research Facilities for  
722 their support and everybody involved at Royal NIOZ who made this expedition possible. We  
723 also want to thank chief bottle washer Rachael Davidson who came especially from New  
724 Zealand (University of Otago) to help us cleaning the myriads of bottles in preparation of our  
725 cruises. We are grateful to the Marine Science and Technology Institute (DEU) in Turkey.  
726 Discussions on board with Kemal Can Bizsel enlightened us on the waters of our  
727 investigation. The comments of our colleague Rob Middag improved this manuscript  
728 considerably. We acknowledge the Dutch funding agency (project number: 822.01.015) of the  
729 national science foundation NWO for funding of this work as part of GEOTRACES and for  
730 funding the PhD research of author Hans Slagter (project number: 822.01.018).

731 The data were collected within the GEOTRACES programme and can be requested at  
732 the British Ocean Data Centre (<http://www.bodc.ac.uk>).

733 Data on Fe species and the dissolved Fe-binding ligands are given in the  
734 Supplementary Table 1

735

736

## 737 **Figure captions**

738 **Figure 1:** Cruise tracks of the Dutch GEOTRACES Section GA04 in the Mediterranean  
739 Sea. The southern cruise (S) (64PE370) is indicated with a red line and red symbols, the  
740 cruise track consists of 37 stations. The part of the southern cruise in the Sea of Marmara is

741 indicated with a green line and green symbols. The northern cruise (N) (64PE374) is indicated  
742 with a blue line and blue symbols, it consists of 19 stations. The stations where Fe-binding  
743 dissolved organic ligands were sampled are indicated by station numbers. Geographical  
744 names used in the main text are indicated. In yellow the occurrence of mud-volcanos is  
745 indicated where these are part of the volcanic active Hellenic and Aeolian Arcs (after Mascle  
746 et al., 2014).

747

748 **Figure 2:** Southern cruise transect showing: A: Absolute Salinity (SA) in  $\text{g kg}^{-1}$ ; B:  
749 Conservative Temperature (CT) in  $^{\circ}\text{C}$ ; C: Density as sigma-theta in  $\text{kg m}^{-3}$ ; D: Oxygen in  $\mu\text{M}$   
750  $\text{kg}^{-3}$ ; E: Fluorescence in  $\mu\text{g dm}^{-3}$ ; F: Attenuation coefficient in  $\text{m}^{-1}$ .  
751 Salinity contours are given every  $0.5 \text{ g kg}^{-1}$  between 36 and 37, and every  $0.1 \text{ g kg}^{-1}$  between  
752 37 and 39.5. Sigma-theta contours are every  $0.5 \text{ kg m}^{-3}$  between 27 and 29.5, every  $0.001 \text{ kg}$   
753  $\text{m}^{-3}$  between 29.1 and 29.120 and between 29.173 and 29.2 and every  $0.002 \text{ kg m}^{-3}$  between  
754 29.2 and 29.26.

755

756 **Figure 3:** Northern cruise transect with A: Absolute Salinity (SA) in  $\text{g kg}^{-1}$ ; B: Conservative  
757 Temperature (CT) in  $^{\circ}\text{C}$ ; C: Density as sigma-theta in  $\text{kg m}^{-3}$ ; D: Oxygen in  $\mu\text{M kg}^{-3}$ ; E:  
758 Fluorescence in  $\mu\text{g dm}^{-3}$ ; F: Attenuation coefficient in  $\text{m}^{-1}$ .  
759 Salinity contours are given every  $0.1 \text{ g kg}^{-1}$  between 37.5 and 39.5. Sigma-theta contours are  
760 every  $0.5 \text{ kg m}^{-3}$  between 27 and 29.5, every  $0.001 \text{ kg m}^{-3}$  between 29.1 and 29.120 and  
761 between 29.173 and 29.2 and every  $0.002 \text{ kg m}^{-3}$  between 29.2 and 29.26.

762

763 **Figure 4:** Transect from the Southern cruise into the Sea of Marmara with A: Absolute  
764 Salinity (SA) in  $\text{g kg}^{-1}$ ; B: Conservative Temperature (CT) in  $^{\circ}\text{C}$ ; C: Oxygen in  $\mu\text{M kg}^{-3}$ ; D:  
765 DFe in nM, E: Fluorescence in  $\mu\text{g dm}^{-3}$ .

766 There is no data available for oxygen at station 36 at 800 m, influencing the  
767 interpretation between stations by ODV.

768 Salinity contours are given every  $2 \text{ g kg}^{-1}$  between 20 and 39.5.

769

770 **Figure 5:** Southern (Figure 5A) and northern (Figure 5B) cruise transect showing DFe in nM.  
771 The southern transect consists of 721 data points, the northern transect consists of 421 data  
772 points. Station 25S was not sampled for DFe (see methods). See Figure 1 for the positions of  
773 the stations.

774

775 **Figure 6:** Dissolved Fe (DFe in nM) with standard deviations (small values falling  
776 within the size of the symbol, see Supplementary Table 1) versus depth (m) of A: stations in  
777 the Atlantic Ocean (AW); B: stations from the southern cruise (S); C: stations from the  
778 northern cruise (N); D: stations from the Sea of Marmara.

779 **Figure 7:** The concentration of Fe-binding dissolved organic ligands with standard  
780 errors ([Lt] in nEq of M Fe, small errors falling within the size of the symbol) versus depth  
781 (m) of A: stations in the Atlantic Ocean (AW); B: stations from the southern cruise (S); C:  
782 stations from the northern cruise (N); D: stations from the Sea of Marmara.

783

784 **Figure 8:** The ratio of Fe-binding dissolved organic ligands ([Lt] in nEq of M Fe) and  
785 dissolved Fe (DFe in nM) versus depth (m) of A: stations in the Atlantic Ocean (AW); B:  
786 stations from the southern cruise (S); C: stations from the northern cruise (N); D: stations  
787 from the Sea of Marmara.

788 Values of samples off scale in the upper 100 m are indicated in figure 8 A.

789

790  
791  
792  
793  
794  
795  
796  
797  
798  
799  
800  
801  
802  
803  
804  
805  
806  
807  
808  
809  
810  
811  
812  
813  
814  
815  
816

Table 1: Concentrations of SAFe and GEOTRACES reference samples in nM kg<sup>-1</sup>.

Columns show reference ID, the Intercalibration Consensus Values (ICV) and the bottle number of GS reference samples, the values measured during the cruises 64PE370 and 64PE374 in the North Atlantic Ocean, the Mediterranean Sea and the Sea of Marmara, including the standard error, and the number of sample analyses. SAFe S is a surface, SAFe D is deep reference sample and GS is a GEOTRACES surface and GD is a GEOTRACES deep reference sample (<http://www.geotraces.org/science/intercalibration>).

**Table 2:** Median values per environment and per depth layer of

**A:** DFe with the inter quartile range (IQR) of the median and the number of samples (N);

**B:** ligand characteristics logK', [Lt], log $\alpha_{FeL}$ , the calculated [Fe'] and the ratio [Lt]/DFe with the inter quartile ranges (IQR) of the median and the numbers of samples (N)

**Supplementary table 1:** Speciation data of the samples in which dissolved Fe-binding ligands were analysed. DFe (nM) with standard deviation (SD) of triplicate measurements. logK' and [Lt] were obtained from speciation measurements and subsequent application of the Langmuir isotherm to the obtained data (Gerringa et al., 2014). The standard errors (SE) of the data relative to the fitted curve are given. Because K' is expressed as logarithm the SE is not symmetrical and lower (down logK' SE) and upper (up logK' SE) SE are both given. The division over the species were obtained from calculations using a spreadsheet (see text in methods for more detail). NA is missing data, NA for the error in logK' means no standard error could be calculated because the fit was not good enough.

## 817 References

- 818 Abualhaija, M.M., Whitby, H., van den Berg, C.M., 2015. Competition between copper and  
819 iron for humic ligands in estuarine waters. *Marine Chemistry*, 172, 46–56.
- 820 Aguilar-Islas, A.M. Wu, J., Rember, R., Johansen, A.M., Shank, L.M., 2010. Dissolution of  
821 aerosol-derived iron in seawater: Leach solution chemistry, aerosol type, and colloidal  
822 iron fraction *Marine Chemistry* 120: 25–33 doi:10.1016/j.marchem.2009.01.011
- 823 Ambar, I., Serra, N., Neves, F., Ferraira, T., 2008. Observations of the Mediterranean  
824 undercurrent and eddies in the Gulf of Cadiz during 2001. *J. Mar. Syst.* 71 (1–2), 195–  
825 220.
- 826 Baker, A.R., Croot, P.L., 2010. Atmospheric and marine controls on aerosol iron solubility in  
827 seawater. *Marine Chemistry* 120, 4–13.
- 828 Baker, A.R. and Jickells, T. D, 2006. Mineral particle size as a control on aerosol iron  
829 solubility, *Geophys. Res. Lett.*, 33, L17608, doi:10.1029/2006GL026557, 2006.
- 830 Barbeau, K., Rue, E., Bruland, K., Butler, A., 2001. Photochemical cycling of iron in the  
831 surface ocean mediated by microbial iron (III)- binding ligands, *Nature*, 413, 409–  
832 413.
- 833 Beaulieu, S.E., Baker, E.T., German, C.R., 2015 Where are the undiscovered hydrothermal  
834 vents on oceanic spreading ridges? *DSR II*, 121: 202–212.
- 835 Beşiktepe, Ş., Sur, H. İ., Özsoy, E., Latif, M. A., Oğuz, T., Ünlüata, Ü., 1994. The circulation  
836 and hydrography of the Marmara Sea. *Progress in Oceanography*, 34, 285–334.
- 837 Bennett, S.A., Achterberg, E.P., Connelly, D.P., Statham, P.J., Fones, G.R., German, C.R.,  
838 2008. The distribution and stabilisation of dissolved Fe in deep-sea hydrothermal  
839 plumes, *Earth Planet. Sci. Lett.*, 270, 157.
- 840 Bonini, M., Mazzarini, F., 2010. Mud volcanoes as potential indicators of regional stress and  
841 pressurized layer depth. *Tectonophysics* 494, 32–47. doi:10.1016/j.tecto.2010.08.006
- 842 Bonnet, S., Guieu, C., 2006. Atmospheric forcing on the annual iron cycle in the western  
843 Mediterranean Sea: A 1-year survey. *J. Geophys. Res.*, 111, C09010,  
844 doi:10.1029/2005JC003213.
- 845 Boyle, E.A., Edmond, J.M., Sholkovitz, E.R., 1977. The mechanism of iron removal in  
846 estuaries. *Geochim. Cosmochim. Acta* 41: 1313–1324.
- 847 Boyd, P.W., Ibsanmi, E., Sander, S.G., Hunter, K.A., and Jackson, G.A., 2010.  
848 Remineralization of upper ocean particles: implications for iron biogeochemistry.  
849 *Limnol. Oceanogr.* 55, 1271–1288.
- 850 Bruland, K.W., Middag, R., Lohan, M.C., 2014. Controls of Trace Metals in Seawater. In:  
851 Holland, H.D., Turekian, K.K., editors. *Treatise on Geochemistry*. Oxford: Elsevier.  
852 pp. 19–51.
- 853 Buck, K.N., Lohan, M.C., Berger, C.J.M., Bruland, K.W., 2007. Dissolved iron speciation in  
854 two distinct river plumes and an estuary: implications for riverine iron supply. *Limnol.*  
855 *Oceanogr.* 52, 843–855.
- 856 Buck, C.S., Landing, W.M., Resing, J.A., Measures, C.I., 2010. The solubility and deposition  
857 of aerosol Fe and other trace elements in the North Atlantic Ocean: Observations from  
858 the A16N CLIVAR/CO2 repeat hydrography section. *Marine Chemistry* 120 (2010)  
859 57–70. doi:10.1016/j.marchem.2008.08.003
- 860 Buck, K.N., Moffett, J.W., Barbeau, K.A.R., Bundy, M. Kondo, Y., Wu, J., 2012. The organic  
861 complexation of iron and copper: an intercomparison of competitive ligand exchange-  
862 adsorptive cathodic stripping voltammetry (CLE-ACSV) techniques. *Limnology and*  
863 *Oceanography: Methods* 10: 496–515.
- 864 Buck, K.N., Sohst, B., Sedwick, P.N., 2015. The organic complexation of dissolved iron  
865 along the U.S.GEOTRACES (GA03) North Atlantic Section. *Deep-Sea Research II*  
866 116(2015)152–165 <http://dx.doi.org/10.1016/j.dsr2.2014.11.016>

867 Buck K.N., Gerringa L.J.A., Rijkenberg M.J.A., 2016. An Intercomparison of Dissolved Iron  
868 Speciation at the Bermuda Atlantic Time-series Study (BATS) Site: Results from  
869 GEOTRACES Crossover Station A. *Front. Mar. Sci.* 3:262. doi:  
870 10.3389/fmars.2016.00262

871 Bundy, R.M., Abdulla, H.A., Hatcher, P.G., Biller, D.V., Buck, K.N. and Barbeau, K.A.,  
872 2015. Iron-binding ligands and humic substances in the San Francisco Bay estuary and  
873 estuarine-influenced shelf regions of coastal California. *Marine Chemistry*, 173, 183-  
874 194.

875 Bundy, R.M., Jiang, M., Carter, M., Barbeau, K.A., 2016. Iron-binding ligands in the  
876 Southern California Current System: Mechanistic studies. *Frontiers in Marine Science*  
877 **3**: Article 27.

878 Butler, A., 2005. Marine siderophores and microbial iron mobilization. *Biometals* 18,369–  
879 374.doi:10.1007/s10534-005-3711-0

880 Croot, P.L., Johansson, M., 2000. Determination of iron speciation by cathodic stripping  
881 voltammetry in seawater using the competing ligand 2-(2-Thiazolylazo)-p-cresol  
882 (TAC). *Electroanalysis*. 12, No.8, 565-576.

883 Croot, P.L., Strey, P., Baker, A.R., 2004 Short residence time for iron in surface seawater  
884 impacted by atmospheric dry deposition from Saharan dust events. *GEOPHYS. RES.*  
885 *LETT.*, 31, L23S08, doi:10.1029/2004GL020153.

886 Dai, M., Martin, J.-M., Cauwet, G., 1995. The significant role of colloids in the transport and  
887 transformation of organic carbon and associated trace metals (Cd, Cu and Ni) in the  
888 Rhône delta (France). *Mar. Chem.* 51: 159–175.

889 de Jong, J., Schoemann, V., Lannuzel, D., Croot, P., De Baar, H., Tison, J.-L., 2012. Natural  
890 iron fertilization of the Atlantic sector of the Southern Ocean by continental shelf  
891 sources of the Antarctic Peninsula. *J. Geophys. Res.* 117, G01029,  
892 doi:10.1029/2011JG001679.

893 Fishwick, M.P., Sedwick, P.N., Lohan, M.C., Worsfold, P.J., Buck, K.N., Church T.M.,  
894 Ussher, S.J., 2014. The impact of changing surface ocean conditions on the dissolution  
895 of aerosol iron. *Glob. Biogeochem. Cycl.*, 28: 1235-1250.

896 Fitzsimmons, J.N., Boyle, E.A., Jenkins, W.J., 2014. Distal transport of dissolved  
897 hydrothermal iron in the deep South Pacific Ocean. *PNAS* 111, 47: 16654–16661.  
898 www.pnas.org/cgi/doi/10.1073/pnas.1418778111

899 Fitzsimmons, J.N., Bundy, R.M., Al-Subiaí, S.N., Barbeau, K.A., Boyle, E.A., 2015. The  
900 composition of dissolved iron in the dusty surface ocean: An exploration using size-  
901 fractionated iron-binding ligands. *Marine Chemistry*, 173: 125–135.  
902 doi.org/10.1016/j.marchem.2014.09.002

903 Gascard, J.-C., 1973. Vertical motions in a region of deep water formation, *Deep Sea Res.*,  
904 20, 1011– 1027.

905 Gerringa, L.J.A., Veldhuis, M.J.W., Timmermans, K.R., Sarthou, G., de Baar, H.J.W., 2006.  
906 Co-variance of dissolved Fe-binding ligands with biological observations in the  
907 Canary Basin. *Mar Chem.*, 102, 276-290. doi:10.1016/j.marchem.2006.05.004

908 Gerringa, L.J.A., Rijkenberg, M.J.A., Wolterbeek, H.Th., Verburg, T., Boye, M., de Baar,  
909 H.J.W., 2007. Kinetic study reveals weak Fe-binding ligand, which affects the  
910 solubility of Fe in the Scheldt estuary. *Mar Chem.* 103, 30-45.  
911 doi:10.1016/j.marchem.2006.06.002

912 Gerringa, L.J.A., Rijkenberg, M.J.A., Thuróczy, C-E., Maas, L.R.M., 2014. A critical look at  
913 the calculation of the binding characteristics and concentration of iron complexing  
914 ligands in seawater with suggested improvements. *Environmental Chemistry* 11, 114-  
915 136..http://dx.doi.org/10.1071/EN13072.

916 Gerringa, L.J.A., Rijkenberg, M.J.A., Schoemann, V., Laan, P., de Baar, H.J.W., 2015.  
917 Organic complexation of iron in the West Atlantic Ocean. *Mar Chem.* 177:434-446.  
918 [.doi.org/10.1016/j.marchem.2015.04.007](https://doi.org/10.1016/j.marchem.2015.04.007)

919 Gerringa, L.J.A., Rijkenberg, M.J.A., Bown, J., Margolin, A.R., Laan, P., de Baar, H.J.W.,  
920 2016. Fe-binding dissolved organic ligands in the oxic and suboxic waters of the  
921 Black Sea. *Front. Mar. Sci.* 3:84. doi: 10.3389/fmars.2016.00084

922 Gledhill, M., McCormack, P., Ussher, S., Achterberg, E.P., Mantoura, R.F.C., Worsfold, P.J.,  
923 2004. Production of siderophore type chelates by mixed bacterioplankton populations  
924 in nutrient enriched seawater incubations. *Mar.Chem.* 88: 75– 83.  
925 doi:10.1016/j.marchem.2004.03.003

926 Gledhill, M., Buck, K.N., 2012. The organic complexation of iron in the marine environment:  
927 a review. *Frontiers in Microbiology* <http://dx.doi.org/10.3389/fmicb.2012.00069>.

928 Gledhill, M., Gerringa, L.J.A. submitted. The effect of metal concentration on the parameters  
929 derived from complexometric titrations of trace elements in seawater – a model study.  
930 Submitted to *Frontiers in Microbiology*

931 Gobler, C.J., Hutchins, D.A., Fisher, N.S., 1997. Release and bioavailability of C, N, P, Se,  
932 and Fe following viral lysis of a marine chrysophyte. *Limnol. Oceanogr.* 42,1492–  
933 1504.doi:10.4319/lo.1997.42.7.1492

934 Guieu, C., Martin, J.-M., Thomas, A.J., Elbaz-Poulichet, F., 1991. Atmospheric Versus River  
935 Inputs of Metals to the Gulf of Lions. *Total Concentrations, Partitioning and Fluxes.*  
936 *Marine Pollution Bulletin, Volume 22:* 176-183.

937 Guieu, C., Chester, R., Nimmo, M., Martin, J.-M., Guerzoni, S., Nicolas, A., Mateu, J.,  
938 Keyset, S., 1997. Atmospheric input of dissolved and particulate metals to the  
939 northwestern Mediterranean. *DSR II*, 44: 655-674. PII: SO967-0645(96)00088-4

940 Guieu, C., Loÿe-Pilot, M.-D., Benyahya, L., Dufour, A., 2010a. Spatial variability of  
941 atmospheric fluxes of metals (Al, Fe, Cd, Zn and Pb) and phosphorus over the whole  
942 Mediterranean from a one-year monitoring experiment: Biogeochemical implications.  
943 *Mar. Chem.*, 120: 164-178.

944 Guieu, C., Dulac, F., Desboeufs, K., Wagener, T., Pulido-Villenal, E., Grisoni, J-M., Louis,  
945 F., Ridame, C., Blain, S., Brunet, C., Bon Nguyen, E., Tran, S., Labiadh, M.,  
946 Dominicil, J-M., 2010b. Large clean mesocosms and simulated dust deposition: a new  
947 methodology to investigate responses of marine oligotrophic ecosystems to  
948 atmospheric inputs. *Biogeosciences*, 7, 2765–2784. doi:10.5194/bg-7-2765-2010

949 Hawkes, J.A., Connelly, D.P., Gledhill, M., Achterberg, E.P., 2013. The stabilisation and  
950 transportation of dissolved iron from high temperature hydrothermal vent systems.  
951 *Earth Plan. Sci.Lett.* 375:280–290.

952 Hatta, M., Measures, C., Wu, J., Roshan, R., Fitzsimmons, J., Sedwick, P., Morton, P., 2015.  
953 An overview of dissolved Fe and Mn distributions during the 2010–2011 U.S.  
954 GEOTRACES north Atlantic cruises: GEOTRACESGA03.Deep-Sea  
955 ResearchIII16(2015)117–129 <http://dx.doi.org/10.1016/j.dsr2.2014.07.005>

956 Heimbürger, L.E., Migon, C., Losno, R., Miquel, J.-C., Thibodeau, B., Stabholz, M., Dufour,  
957 A., Leblond, N., 2014. Vertical export flux of metals in the Mediterranean Sea. *Deep-*  
958 *Sea Research I*, 87: 14–23..doi/10.1016/j.dsr.2014.02.001

959 Hudson, R.J.M., Covault, D.T. Morel, F.M.M., 1992. Investigations of iron coordination and  
960 redox reactions in seawater using <sup>59</sup>Fe radiometry and ion-pair solvent extraction of  
961 amphiphilic iron complexes. *Mar. Chem.* 38: 209-235.

962 Hudson, R.J.M., Rue, E.L., Bruland, K.W., 2003. Modeling complexometric titrations of  
963 natural water samples, *Environ. Sci. Techn.* 37, 1553.

964 Hopkinson, B.M., Barbeau, K.A., 2007. Organic and redox speciation of iron in the eastern  
965 tropical North Pacific suboxic zone *Marine Chemistry* 106, 2–17.  
966 doi:10.1016/j.marchem.2006.02.008

967 IOC, SCOR, IAPSO, 2010. The international thermodynamic equation of seawater – 2010:  
968 Calculation and use of thermodynamic properties. Intergovernmental Oceanographic  
969 Commission, Manuals and Guides No. 56, UNESCO, Paris, France, 196 pp.

970 Johansen, A.M., Siefert, R.L., Hoffmann, M.R., 2000. Chemical composition of aerosols  
971 collected over the tropical North Atlantic Ocean. *Journal of Geophysical Research-*  
972 *Atmospheres* 105, 15277-15312.

973 Johnson, K.S., Boyle, E., Bruland, K., Measures, C., Moffett, J., Aquilarislas, A., Barbeau,  
974 K., Cai, Y., Chase, Z., Cullen, J., Doi, T., Elrod, V., Fitzwater, S., Gordon, M., King,  
975 A., Laan, P., Laglera-Baquer, L., Landing, W., Lohan, M., Mendez, J., Milne, A.,  
976 Obata, H., Ossiander, L., Plant, J., Sarthou, G., Sedwick, P., Smith G.J., Sohst, B.,  
977 Tanner, S., Van Den Berg, S., Wu, J., 2007. Developing standards for dissolved iron in  
978 seawater. *Eos Trans.* 88, 131.

979 Jones, M.E., Beckler, J.S., Taillefert, M., 2011. The flux of soluble organic- iron(III)  
980 complexes from sediments represents a source of stable iron(III) to estuarine waters  
981 and to the continental shelf. *Limnol.Oceanogr.* 56,1811–1823.  
982 doi:10.4319/lo.2011.56.5.1811

983 Journet, E., Desboeufs, K.V., Caquineau, S., Colin, J.L., 2008. Mineralogy as a critical factor  
984 of dust iron solubility. *Geophys. Res. Lett.* 35, L07805. doi:10.1029/2007GL031589.

985 King, A. L., Buck, K.N., Barbeau, K.A., 2012. Quasi-Lagrangian drifter studies of iron  
986 speciation and cycling off Point Conception, California. *Mar. Chem.* 128-129: 1-12.

987 Kleint, C., Hawkes J.A., Sander S.G., Koschinsky, A., 2016. Voltammetric Investigation of  
988 Hydrothermal Iron Speciation. *Front. Mar. Sci.* 3:75. doi: 10.3389/fmars.2016.00075.

989 Klunder, M.B., Laan, P., Middag, R., de Baar, H.J.W., van Ooijen, J.C., 2011. Dissolved Fe  
990 in the Southern Ocean (Atlantic sector). *DSR. II* 58, 2678-2694.

991 Klunder, M. B., Laan, P., Middag, R., de Baar, H. J. W., Bakker, K., 2012. Dissolved iron in  
992 the Arctic Ocean: Important role of hydrothermal sources, shelf input and scavenging  
993 removal, *J. Geophys. Res.*, 117, C04014, doi:10.1029/2011JC007135.

994 Koron, N., Ogrinc, N., Metzger, E., Riedel, B., Faganeli, J. 2015. The impact of reduced  
995 redox transitions on nutrient diagenesis in coastal marine sediments (Gulf of Trieste,  
996 northern Adriatic Sea). *J. Soils Sediments*: 1491-1518, DOI 10.1007/s11368-0151215-  
997 2

998 Laglera, L.M., Battaglia, G., Van Den Berg, C.M.G., 2011. Effect of humic substances on the  
999 iron speciation in natural waters by CLE/CSV. *Mar. Chem.* 127, 134–143.

1000 Laglera, L. M., Downes, J., Santos-Echeandía, J., 2013. Comparison and combined use of  
1001 linear and non-linear fitting for the estimation of complexing parameters from metal  
1002 titrations of estuarine samples by CLE/AdCSV. *Mar. Chem.* 155: 102-112.

1003 Lazar, C.S., Parkes, R.J., Cragg, B.A., L' Haridon, S.L., Toffin, L., 2012. Methanogenic  
1004 activity and diversity in the centre of the Amsterdam Mud Volcano, Eastern  
1005 Mediterranean Sea. *FEMS Microbiol Ecol* 81, 243–254. DOI: 10.1111/j.1574-  
1006 6941.2012.01375.x

1007 Liu, X., Millero, F.J., 2002. The solubility of iron in seawater. *Mar. Chem.* 77, 43–54.

1008 Lupton, J., de Ronde, C., Spovieri, M., Baker, E.T., Bruno, P.P., Italiano, F., Walker, S.,  
1009 Faure, K., Leybourne, M., Britten, K., Greene, R., 2011. Active hydrothermal  
1010 discharge on the submarine Aeolian Arc. *J. Geophys. Res.*, 116, B02102,  
1011 doi:10.1029/2010JB007738.

1012 Mahmood, A., Abualhaija, M.M., van den Berg, C.M.G., Sander, S.G., 2015. Organic  
1013 speciation of dissolved iron in estuarine and coastal waters at multiple analytical  
1014 windows. *Marine Chemistry* 177: 706–719

1015 Mascle, J., Mary, F., Praeg, D., Brosolo, L., Camera, L., Ceramicola, S., Dupré, S., 2014.  
1016 Distribution and geological control of mud volcanoes and other fluid/free gas seepage  
1017 features in the Mediterranean Sea and nearby Gulf of Cadiz. *Geo-Marine Letters* June  
1018 2014, Volume 34, Issue 2-3, Pages 89-110. doi.org/10.1007/s00367-014-0356-4

1019 Middag, R., Séférian, R., Conway, T.M. John, S.G., Bruland, K.W., de Baar, H.J.W., 2015.  
1020 Intercomparison of dissolved trace elements at the Bermuda Atlantic Time Series  
1021 station. *Marine Chemistry*, 177: 476–489. doi.org/10.1016/j.marchem.2015.06.014

1022 Millot, C., 1999; Circulation in the Western Mediterranean Sea. *Journal of Marine Systems* 20  
1023 \_1999. 423–442. PII: S0924- 7963\_98.00078-5

1024 Millot, C., Taupier-Letage, I., 2005. Circulation in the Mediterranean Sea, in: *Handbook of*  
1025 *Environmental Chemistry*, vol. 5, part K, edited by A. Saliot, pp. 29– 66, Springer,  
1026 New York.

1027 Nomikou, P., Papanikolaou, D., Alexandri, M., Sakellariou, D., Rousakis, G., 2013.  
1028 Submarine volcanoes along the Aegean volcanic arc. *Tectonophysics* 597–598 (2013)  
1029 123–146. DOI: 10.1016/j.tecto.2012.10.001

1030 Omoregie, E.O., Mastalerz, V., de Lange, G., Straub, .L., Kappler A., Røy, H., Stadnitskaia,  
1031 A., Foucher, J-P., Boetius, A., 2008. Biogeochemistry and Community Composition  
1032 of Iron- and Sulfur-Precipitating Microbial Mats at the Chefren Mud Volcano (Nile  
1033 Deep Sea Fan, Eastern Mediterranean). *Appl. Environm. Microbiol.*, 74, 3198–3215.  
1034 doi:10.1128/AEM.01751-07

1035 Paris, R., Desboeufs, K.V., Journet, E., 2011. Variability of dust iron solubility in atmospheric  
1036 waters: Investigation of the role of oxalate organic complexation. *Atmospheric*  
1037 *Environment* 45, 6510-6517.

1038 Paucot, H., Wollast, R., 1997. Transport and transformation of trace metals in the Scheldt  
1039 estuary. *Mar. Chem.* 58, 229–244.

1040 Pekey, H., 2006. The distribution and sources of heavy metals in Izmit Bay surface sediments  
1041 affected by a polluted stream. *Marine Pollution Bulletin* 52 (2006) 1197–1208.  
1042 doi:10.1016/j.marpolbul.2006.02.012

1043 Pollak, M.J., 1951: The sources of the deep water in the Eastern Mediterranean. *Journal of*  
1044 *Marine Research*, 10, 128-152.

1045 Poorvin, L., Sander, S. G., Velasquez, Ibisani, E., Le Cleir, G. R., Wilhelm, S. W., 2011. A  
1046 comparison of Fe bioavailability and binding of a catecholate siderophores with virus-  
1047 mediated lysates from the marine bacterium *Vibrio alginolyticus* PWH3a. *J. Exp. Mar.*  
1048 *Biol. Ecol.* 399, 43–47. doi: 10.1016/j.jembe.2011.01.016

1049 Powell, R.T., Wilson-Finelli, A., 2003. Photochemical degradation of organic iron  
1050 complexing ligands in seawater. *Aquat. Sci.* 65 (2003) 367–374. DOI 10.1007/s00027-  
1051 003-0679-0

1052 Pižeta, I., Sander, S.G., Hudson, R.J.M., Baars, O., Barbeau, K.A., Buck, K.N., Bundy R.M.,  
1053 Carrasco, G., Croot, P. L., Garnier, C., Gerringa, L.J.A., Gledhill, M., Hirose, K.,  
1054 Kondo, Y., Laglera, L.M., Nuester, J., Omanović, D., Rijkenberg, M.J.A., Takeda, S.,  
1055 Twining, B.S., Wells, M., 2015. Quantitative analysis of complexometric titration  
1056 data: An intercomparison of methods for estimating models of metal complexation by  
1057 mixtures of natural ligands. *Mar Chem*, 173: 3-24.

1058 Press, W.H., Flannery, B.P., Teukolsky, S.A., Vetterling, W.T., 1986. Root finding and  
1059 nonlinear sets of equations, in *Numerical Recipes*, pp. 347–393 (Cambridge University  
1060 Press: Cambridge, UK).



- 1061 Rodney T., Powell, R.T., Wilson-Finelli, A., 2003. Importance of organic Fe complexing  
 1062 ligands in the Mississippi River plume. *Est. Coast.Shelf Sci.* 58: 757–763.  
 1063 doi:10.1016/S0272-7714(03)00182-3
- 1064 Puig, P., Durrieu de Madron, X., Salat, J., Schroede, K., Martín, J., Karageorgis, A.P.,  
 1065 Palanques, A., Roullier, F., Lopez-Jurado, J.L., Emelianov, M., Moutin, T., Houpert,  
 1066 L., 2013. Thick bottom nepheloid layers in the western Mediterranean generated by  
 1067 deep dense shelf water cascading. *Progress in Oceanography* 111, 1–23.  
 1068 doi.org/10.1016/j.pocean.2012.10.003
- 1069 Rank, D., Özsoy, E., Salihoğlu, İ., 1999. Oxygen-18, deuterium and tritium in the Black Sea  
 1070 and the Sea of Marmara. *Environmental Radioactivity* 43, 231-245. PII: S0265-  
 1071 931X(98)00094-0
- 1072 Rodellas, V., Garcia-Orellana, J., Masqué, P., Feldman, M., Weinstein, Y., 2015. Submarine  
 1073 groundwater discharge as a major source of nutrients to the Mediterranean Sea.  
 1074 *Proceedings of the National Academy of Sciences* 112, 3926-3930.  
 1075 doi/10.1073/pnas.1419049112
- 1076 Roether, W., Klein, B., Bruno Manca, B., Theocharis, A., Kioroglou, S., 2007. Transient  
 1077 Eastern Mediterranean deep waters in response to the massive dense-water output of  
 1078 the Aegean Sea in the 1990s. *Progress in Oceanography* 74, 540–571.  
 1079 doi:10.1016/j.pocean.2007.03.001
- 1080 Rolison, J.M., Middag, R., Stirling, C.H., Rijkenberg, M.J.A., de Baar, H.J.W., 2015. Zonal  
 1081 distribution of dissolved aluminium in the Mediterranean Sea. *Marine Chemistry* 177,  
 1082 Part 1, 87-100.
- 1083 Rue, E.L., Bruland, K.W., 1995. Complexation of iron(III) by natural organic ligands in the  
 1084 Central North Pacific as determined by a new competitive ligand  
 1085 equilibration/adsorptive cathodic stripping voltammetric method. *Mar. Chem.* 50,  
 1086 117–138.
- 1087 Rijkenberg M.J.A., Powell C.F., Dall’Osto M., Nielsdottir M.C., Patey M.D., Hill, P.G.,  
 1088 Baker, A.R., Jickells, T.D. Harrison, R.M., Achterberg, E.P., 2008. Changes in iron  
 1089 speciation following a Saharan dust event in the tropical North Atlantic Ocean. *Mar*  
 1090 *Chem* 110: 56–67.
- 1091 Rijkenberg, M. J. A., Steigenberger, S., Powell, C. F., van Haren, H., Patey, M.D., Baker,  
 1092 A.R., Achterberg, E.P., 2012. Fluxes and distribution of dissolved iron in the eastern  
 1093 (sub-) tropical North Atlantic Ocean, *Global Biogeochem. Cycles*, 26, GB3004,  
 1094 doi:10.1029/2011GB004264.
- 1095 Rijkenberg, M.J.A., Middag, R., Laan, P., Gerringa, L.J.A., van Aken, H., Schoemann, V., de  
 1096 Jong, J.T.M., de Baar, H.J.W., 2014. The distribution of dissolved iron in the West  
 1097 Atlantic Ocean. *PLoS ONE* 9(6): e101323. doi:10.1371/journal.pone.0101323
- 1098 Rijkenberg, M.J.A., de Baar, H.J.W, Bakker, K., Gerringa, L.J.A., Keijzer, E., Laan, M.,  
 1099 Laan, P., Middag, R., Ober, S., Smit, M.G., 2015. “PRISTINE”, a new high volume  
 1100 sampler for ultraclean sampling of trace metals and isotopes. *Mar. Chem.* 177, 501-  
 1101 509.
- 1102 Sander, S.G., Koschinsky, A., 2011. Metal flux from hydrothermal vents increased by organic  
 1103 complexation. *Nat. Geosci.* 4, 145–150.
- 1104 Sarthou, G., Jeandel, C., 2001, Seasonal variations of iron concentrations in the Ligurian Sea  
 1105 and, iron budget in the Western Mediterranean Sea. *Mar. Chem.* 74(2-3): 115-129.
- 1106 Sarthou, G., Baker, A., Kramer, J., Laan, P., Laës, A., Ussher, S., Achterberg, E., de Baar,  
 1107 H.J.W., Timmermans, K.R., Blain, S., 2007. Influence of atmospheric inputs on the  
 1108 iron distribution in the subtropical North-East Atlantic Ocean, *Mar. Chem.*, 104, 186-  
 1109 202 doi:10.1016/j.marchem.2006.11.004

1110 Saydam, A.C., Senyuva, H.Z., 2002. Deserts: Can they be the potential suppliers of  
1111 bioavailable iron? *Geophys. Res. Lett.* 29.

1112 Schlitzer, R., Ocean Data View, <http://odv.awi.de>, 2016.

1113 Schroeder, K., Taillandier, V., Vetrano, A., Gasparini, G.P., 2008. The circulation of the  
1114 western Mediterranean Sea in spring 2005 as inferred from observations and from  
1115 model outputs. *Deep-Sea Research I* 55, 947– 965. doi:10.1016/j.dsr.2008.04.003

1116 Sedwick, P.N., Church, T.M., Bowie, A.R., Marsay, C.M., Ussher, S.J., Achilles, K.M.,  
1117 Lethaby, P.J., Johnson, R.J., Sarin, M.M., McGillicuddy, D.J., 2005 Iron in the  
1118 Sargasso Sea (Bermuda Atlantic Time-series Study region) during summer: Eolian  
1119 imprint, spatiotemporal variability, and ecological implications. *Glob. Biogeochem.*  
1120 *Cycl.*, VOL. 19, 1-11. GB4006, doi:10.1029/2004GB002445.

1121 Sedwick, P.N., Sholkovitz, E.R., Church, T.M., 2007. Impact of anthropogenic combustion  
1122 emissions on the fractional solubility of aerosol iron: evidence from the Sargasso Sea.  
1123 *Geochem. Geophys. Geosyst.* 8, (10), 1-21. doi.org/10.1029/2007GC001586.

1124 Sedwick, P.N., Sohst, B.M., Ussher, S.J., Bowie, A.R., 2015. A zonal picture of the water  
1125 column distribution of dissolved iron(II) during the U.S. GEOTRACES North Atlantic  
1126 transect cruise (GEOTRACESGA03). *Deep-Sea Res. II*, 116, 166–175.  
1127 <http://dx.doi.org/10.1016/j.dsr2.2014.11.004>

1128 Sholkovitz, E.R., 1976. Flocculation of dissolved organic and inorganic matter during the  
1129 mixing of river and seawater. *Geochim. Cosmochim. Acta* 40, 831–845.

1130 Sholkovitz, E. R., 1993. The geochemistry of rare earth elements in the Amazon River  
1131 estuary. *Geochim. Cosmochim. Acta* 57, 2181–2190.

1132 Slagter, H.A., Gerringa, L.J.A., Brussaard, C.P.D., 2016. Phytoplankton Virus Production  
1133 Negatively Affected by Iron Limitation. *Front. Mar. Sci.* 3:156. doi:  
1134 10.3389/fmars.2016.00156

1135 Spokes, L.J., Jickells, T.D., 1996. Factors controlling the solubility of aerosol trace metals in  
1136 the atmosphere and on mixing into seawater. *Aq. Geochem.* 1, 355–374.

1137 Tachikawa, K., Roy-Barman, M., Michard, A., Thouron, D., Yeghicheyan, D., Jeandel, C.,  
1138 2004. Neodymium isotopes in the Mediterranean Sea: Comparison between seawater  
1139 and sediment signals. *Geochim. Cosmochim. Acta*, 68, 3095–3106.  
1140 doi:10.1016/j.gca.2004.01.024

1141 Tagliabue, A., Bopp, L., Dutay, J.C., Bowie, A.R., Chever, F., Jean-Baptiste, P., Bucciarelli,  
1142 E., Lannuzel, D., Remenyi, T., Sarthou, G., Aumont, O., Gehlen, M., Jeandel, C.,  
1143 2010. Hydrothermal contribution to the oceanic dissolved iron inventory. *Nature*  
1144 *Geoscience* 3: 252–256. DOI: 10.1038/NGEO818

1145 Testor, P., Gascard, J.-C., 2003. Large-scale spreading of deep waters in the western  
1146 Mediterranean Sea by submesoscale coherent eddies, *J. Phys. Oceanogr.*, 33, 75– 87.

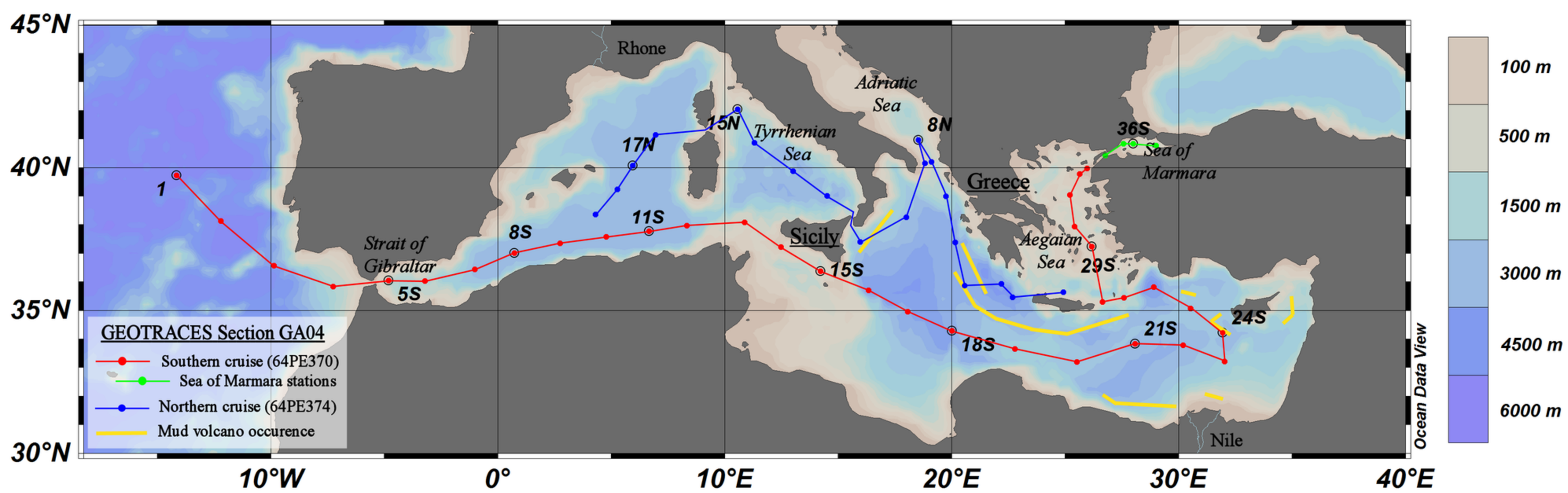
1147 Town, R. M., and Filella, M., 2000. Dispelling the myths: Is the existence of L1 and L2  
1148 ligands necessary to explain metal ion speciation in natural waters? *Limnol. Oceanogr.*  
1149 45, 1341–1357.

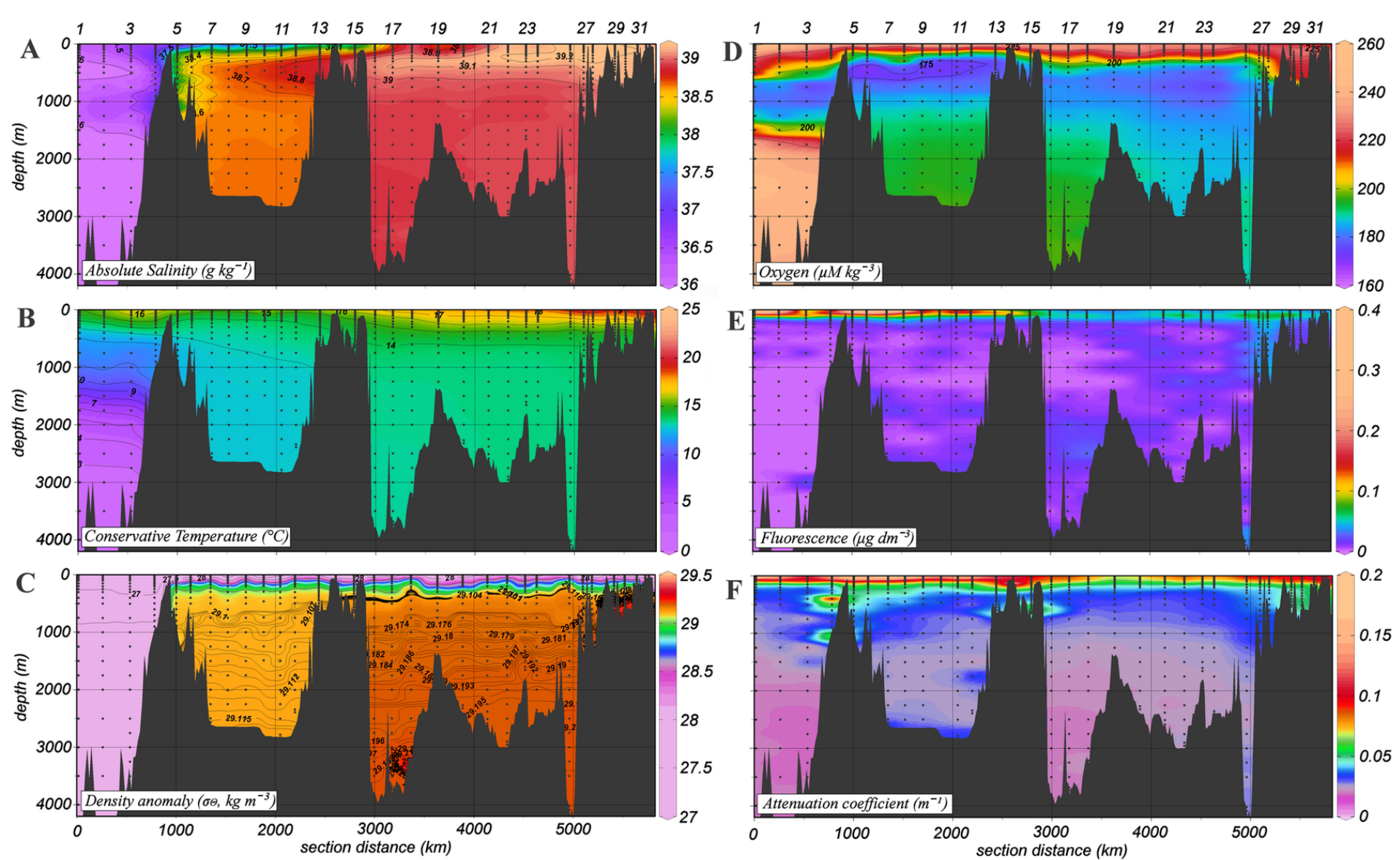
1150 Thuróczy, C.-E., Gerringa, L.J.A., Klunder, M., Middag, R., Laan, P., Timmermans, K.R., de  
1151 Baar, H.J.W., 2010. Speciation of Fe in the North East Atlantic Ocean. *DSR. I*, 57,  
1152 1444-1453.

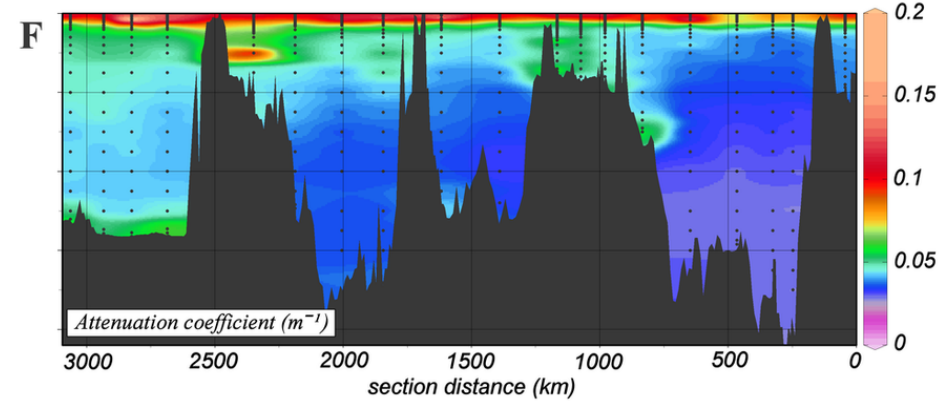
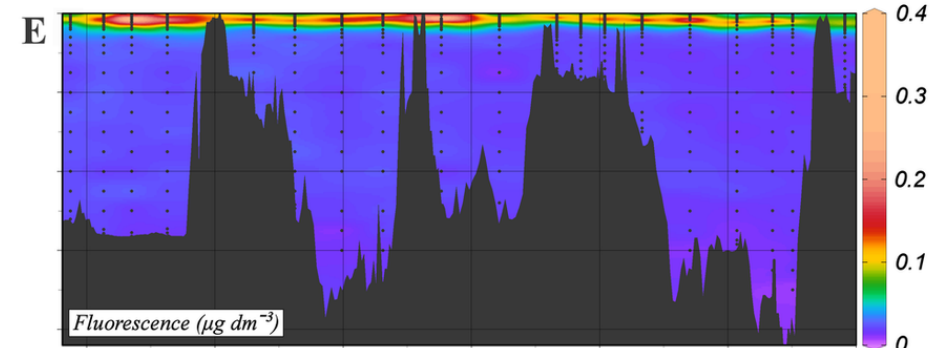
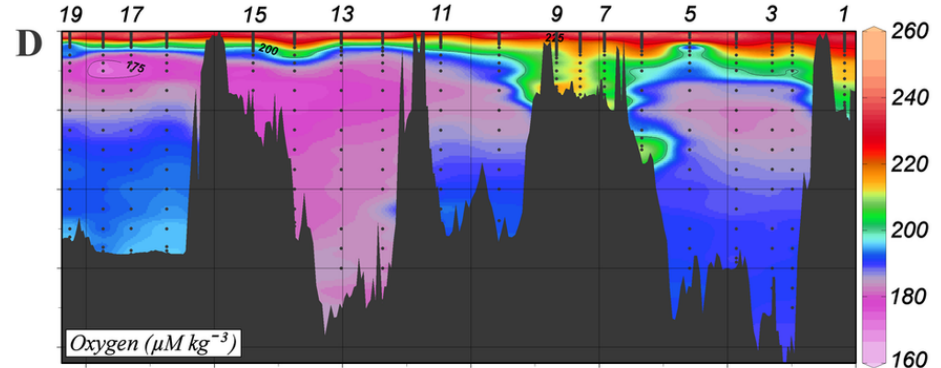
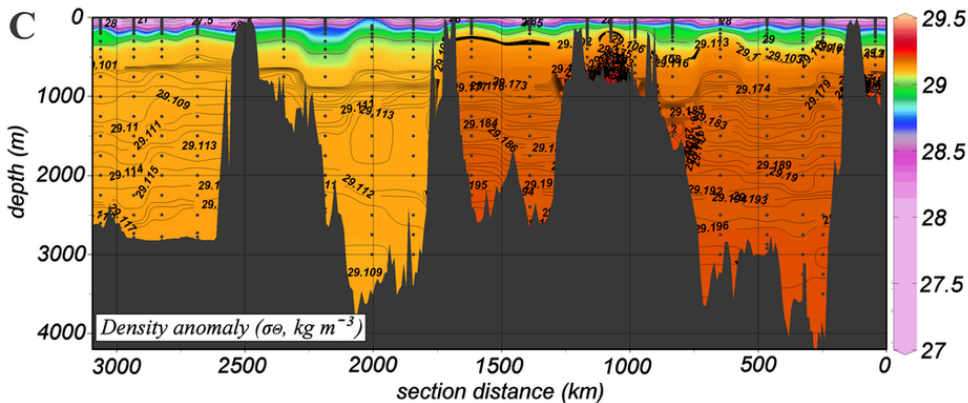
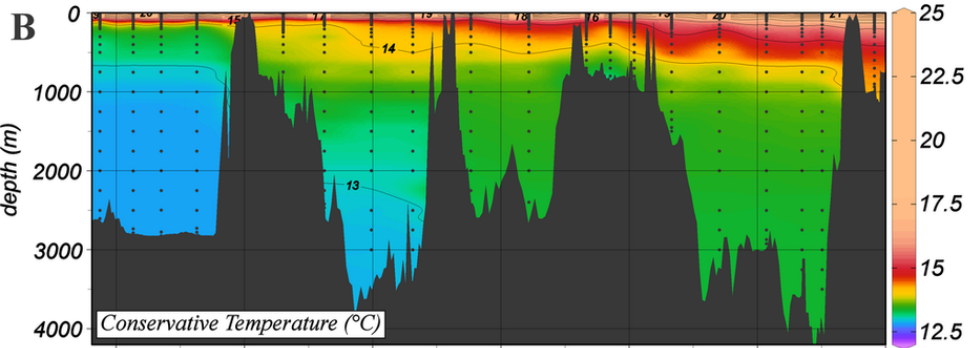
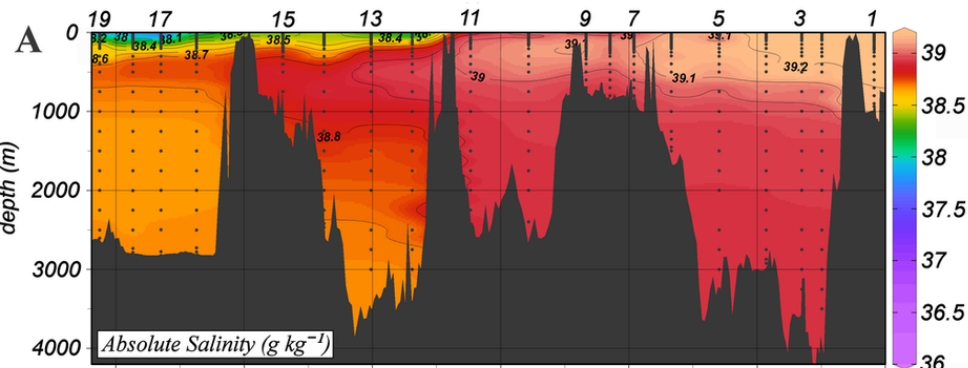
1153 Thuróczy, C.-E., Gerringa, L.J.A., Klunder, M., Laan, P., le Guitton, M., de Baar, H.J.W.,  
1154 2011. Distinct trends in the speciation of iron between the shelf seas and the deep  
1155 basins of the Arctic Ocean. *J. Geophys. Res.*, VOL. 116, C10009, doi:  
1156 10.1029/2010JC006835.

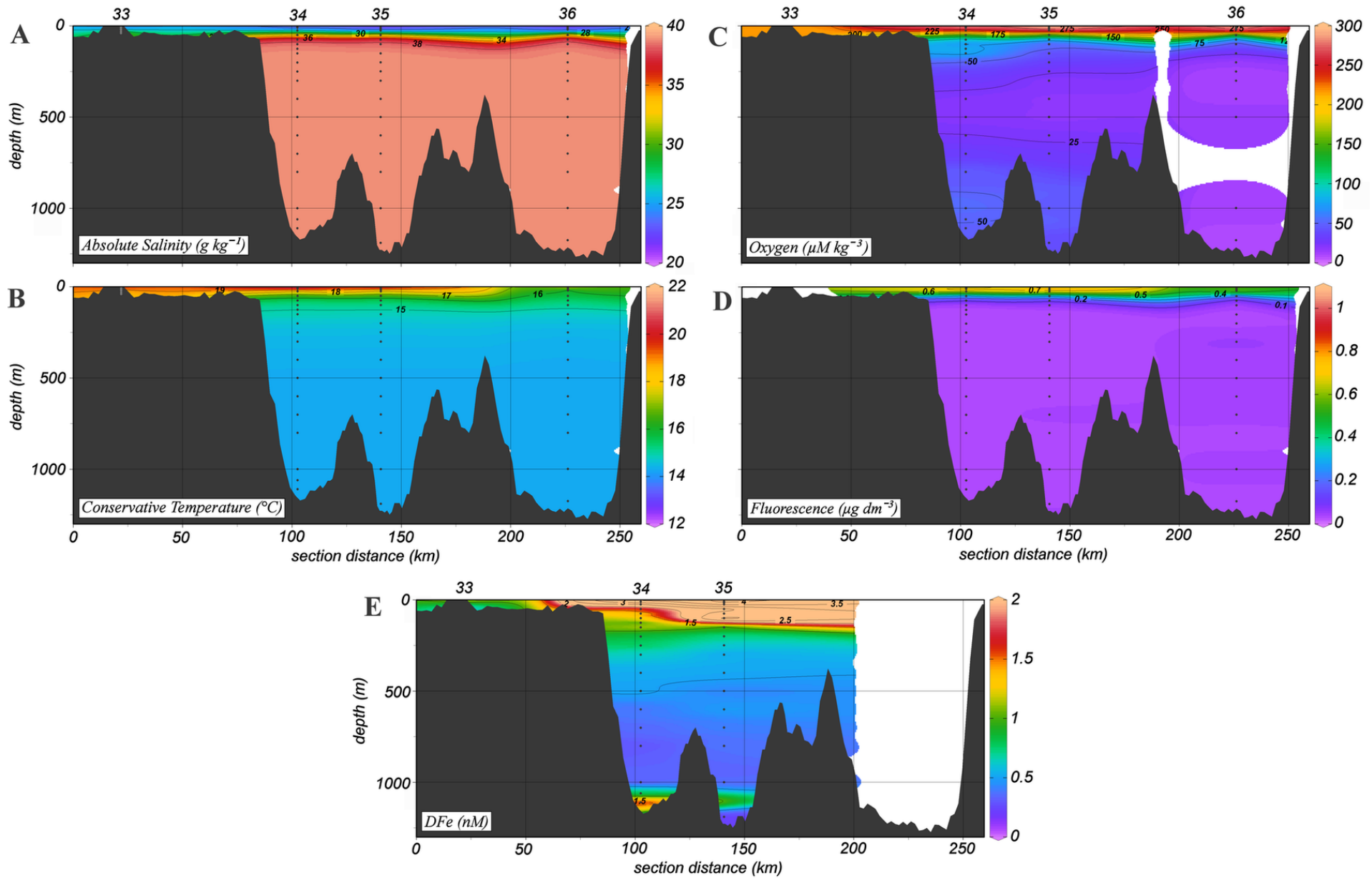
1157 Trezzi, G., Garcia-Orellana, J., Rodellas, V., Santos-Exheandia, J., Tovar-Sanchez, A.,  
1158 Garcia-Solsona, E., Masque, P., 2016. Submarine groundwater discharge: A

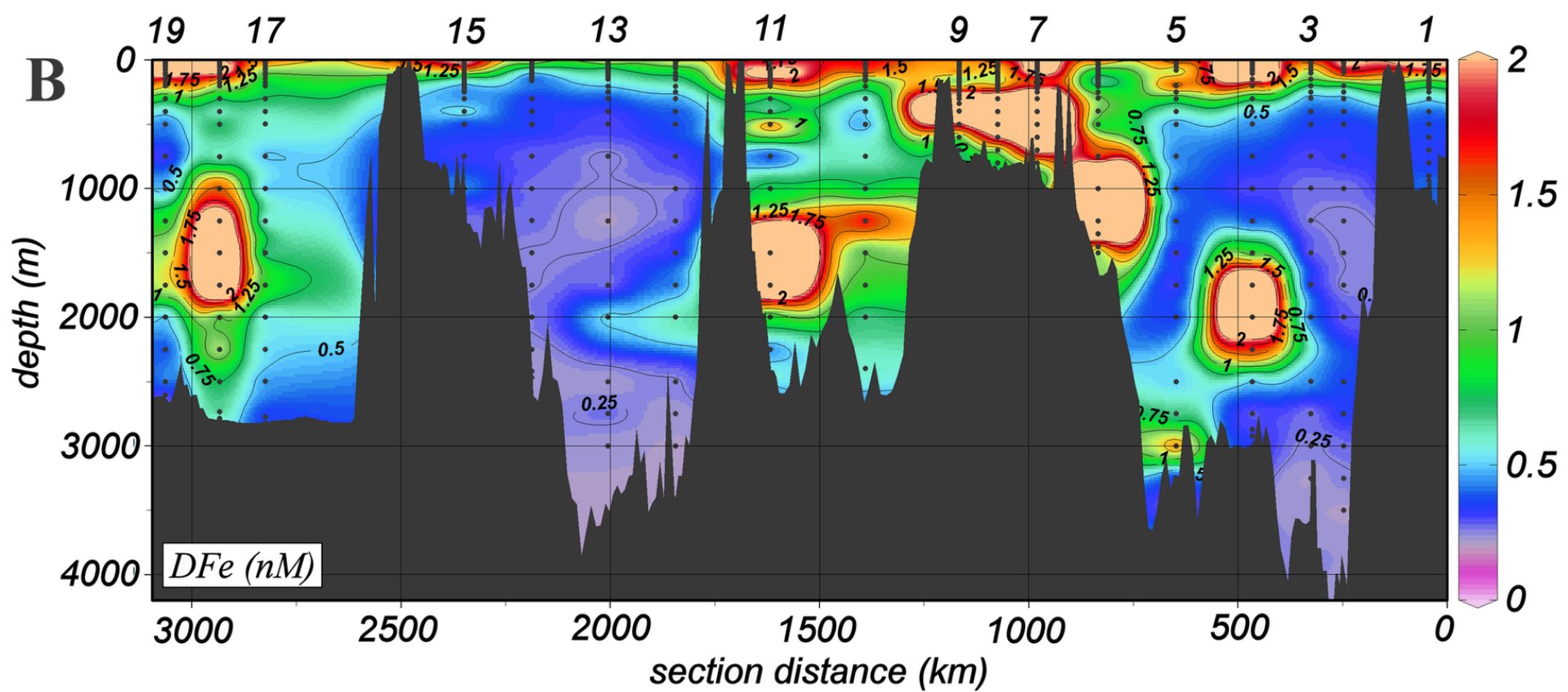
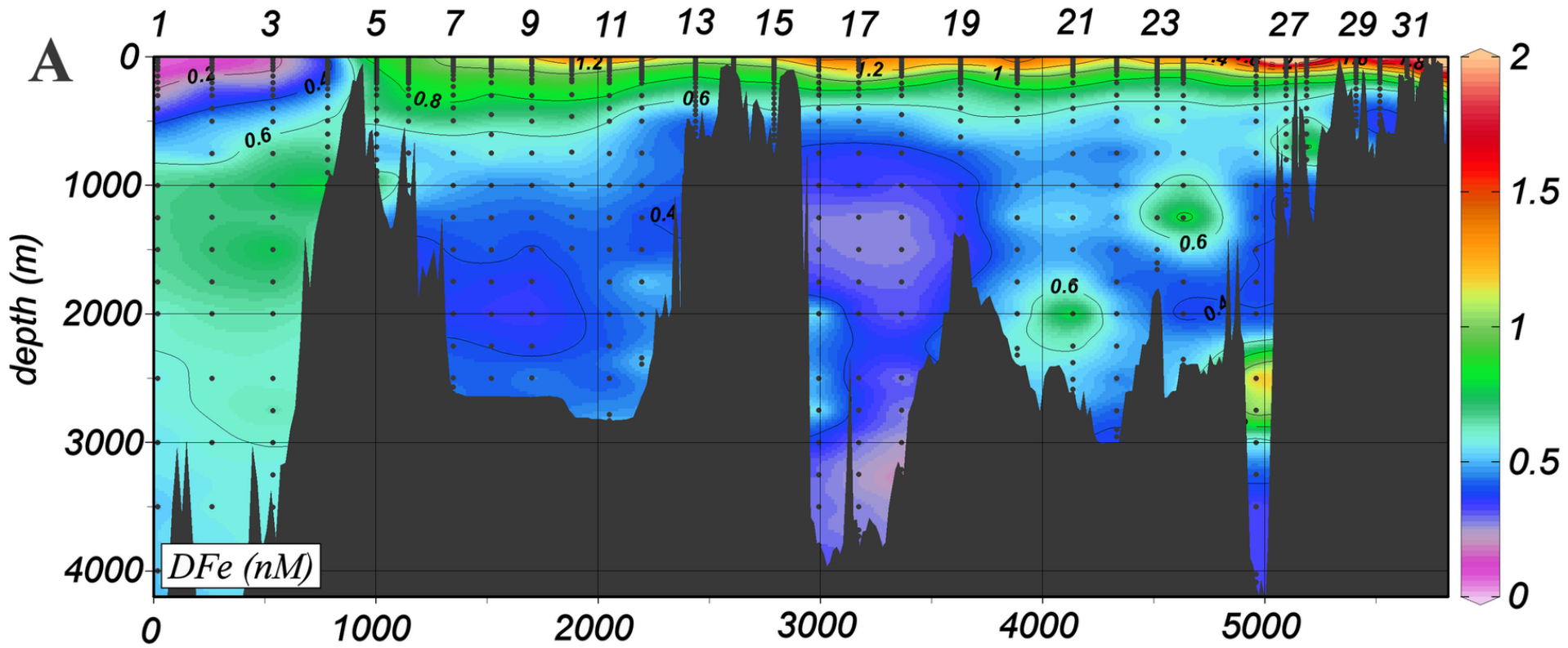
1159 significant source of dissolved trace metals to the North Western Mediterranean Sea.  
 1160 Mar. Chem. 186, 90-100. doi.org/10.1016/j.marchem.2016.08.004  
 1161 Ünlüata, Ü., Oğuz, T., Latif, M. A., Özsoy, E., 1990. On the physical oceanography of the  
 1162 Turkish straits. In Pratt, L. J. (Ed.), The physical oceanography of sea straits (pp. 25-  
 1163 60). NATO/ASI Series. Dordrecht: Kluwer.  
 1164 Van den Berg, C.M.G., 1995. Evidence for organic complexation of iron in seawater. Marine  
 1165 Chemistry 50, 139-157.  
 1166 Van der Poll, W.H., Boute, P.G., Rozema, P.D., Buma, A.G.J., Kulk, G., Rijkenberg, M.J.A.,  
 1167 2015. Sea surface temperature control of taxon specific phytoplankton production  
 1168 along an oligotrophic gradient in the Mediterranean Sea. Mar. Chem. 177, 536–544.  
 1169 doi.org/10.1016/j.marchem.2015.08.005  
 1170 van Haren, H., Millot, C., 2009. Slantwise convection: A candidate for homogenization of  
 1171 deep newly formed dense waters, Geophys. Res. Lett., 36, L12604,  
 1172 doi:10.1029/2009GL038736.  
 1173 van Haren, H., Millot, C., Taupier-Letage, I., 2006. Fast deep sinking in Mediterranean  
 1174 eddies. Geophys. Res. Lett., 33, L04606, doi: 10. 1029/ 2005GL025367.  
 1175 van Haren, H. et al. (ANTARES Collaboration), 2014. High-frequency internal wave motions  
 1176 at the ANTARES site in the deep Western Mediterranean. Ocean Dyn., 64, 507-517.  
 1177 Visser, F., Gerringa, L.J.A., van der Gaast, S.J., de Baar, H.J.W., Timmermans, K.R., 2003.  
 1178 The role of reactivity and iron content of aerosol dust on growth rates of two Antarctic  
 1179 diatom species. J. Phycol. 39, 1085-1094.  
 1180 Voorhis, A. D., Webb, D. C., 1970. Large vertical currents observed in a winter sinking  
 1181 region of the northwestern Mediterranean, Cah. Oceanogr. 22, 571–580.  
 1182 Wagener, T., Pulido-Villena, E., Guieu, C., 2008. Dust iron dissolution in seawater: results  
 1183 from a one-year time-series in the Mediterranean Sea. Geophys. Res. Lett. 35, L16601.  
 1184 Wagener, T., Guieu, C., Leblond, N., 2010. Effects of dust deposition on iron cycle in the  
 1185 surface Mediterranean Sea: results from a mesocosm seeding experiment.  
 1186 Biogeosciences 7: 3769- 3781. Doi:10.5194/bg-7-3769-2010.  
 1187 Wozniak, A.S., Shelley, R.U., McElhemie, S.D., Landing, W.M., Hatcher, P.G., 2015.  
 1188 Aerosol water soluble organic matter characteristics over the North Atlantic Ocean:  
 1189 Implications for iron-binding ligands and iron solubility. Marine Chemistry 173: 162–  
 1190 172. doi.org/10.1016/j.marchem.2014.11.002  
 1191 Wu, J., Boyle, E., Sunda, W., Wen, L.-S., 2001. Soluble and colloidal iron in the oligotrophic  
 1192 North Atlantic and North Pacific. Science 293 (5531), 847–849.  
 1193 Zitter, T.A.C., 2004. Mud volcanism and fluid emissions in Eastern Mediterranean  
 1194 neotectonic zones. Applied geology. PhD thesis Vrije Universiteit, Amsterdam 2004,  
 1195 140 pages. This is a Netherlands Research School of Sedimentary Geology (NSG)  
 1196 publication. ISBN 90-9017859-7  
 1197



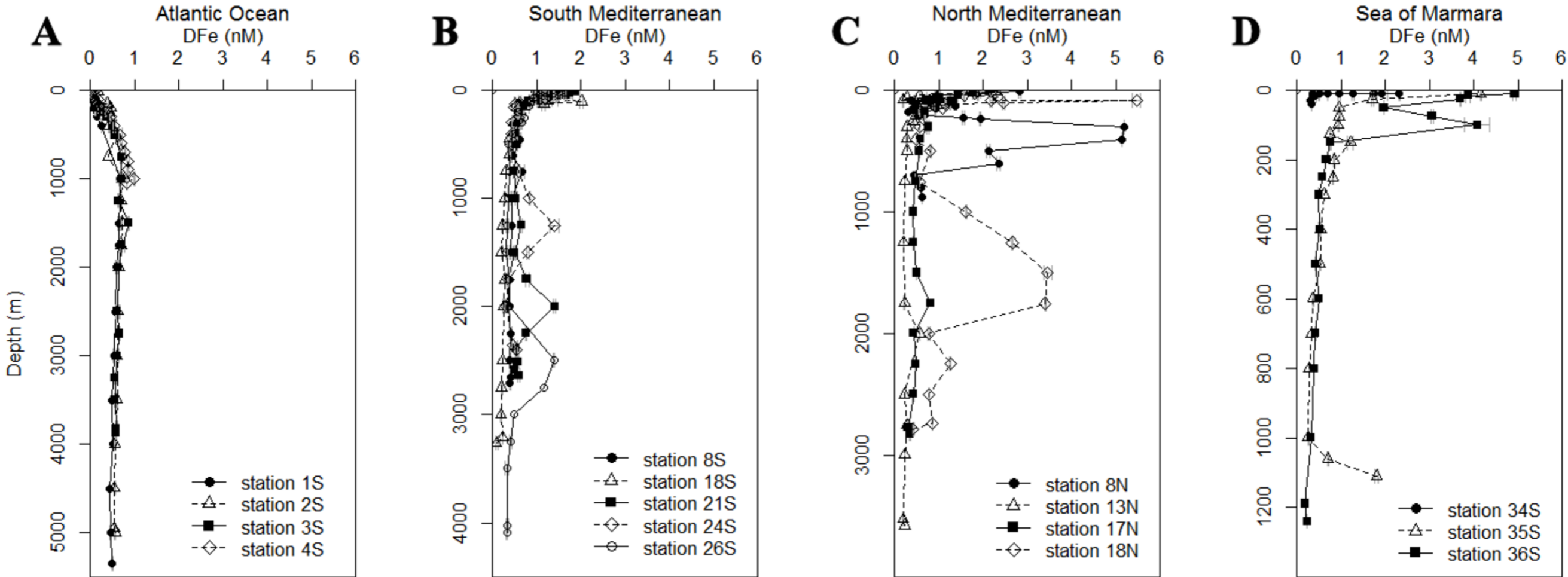


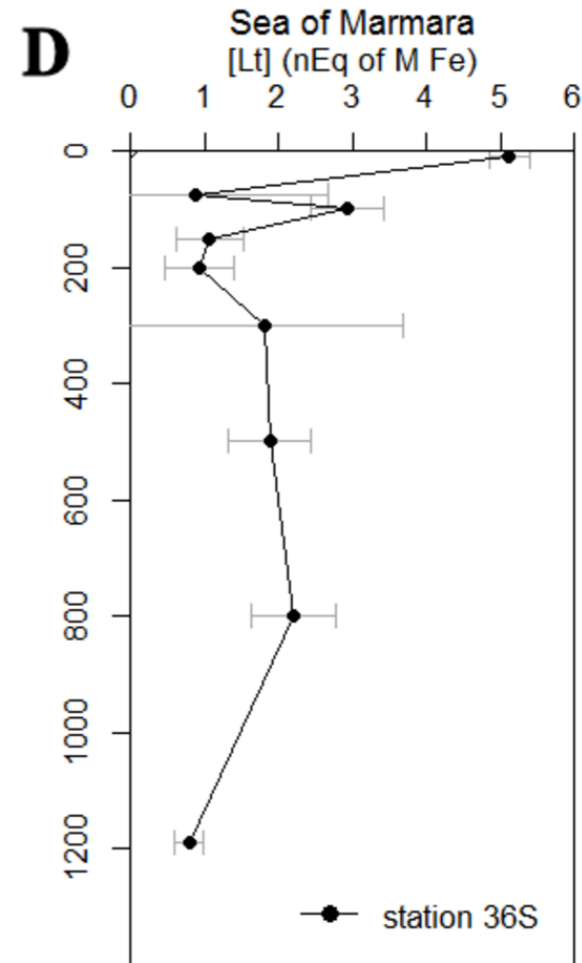
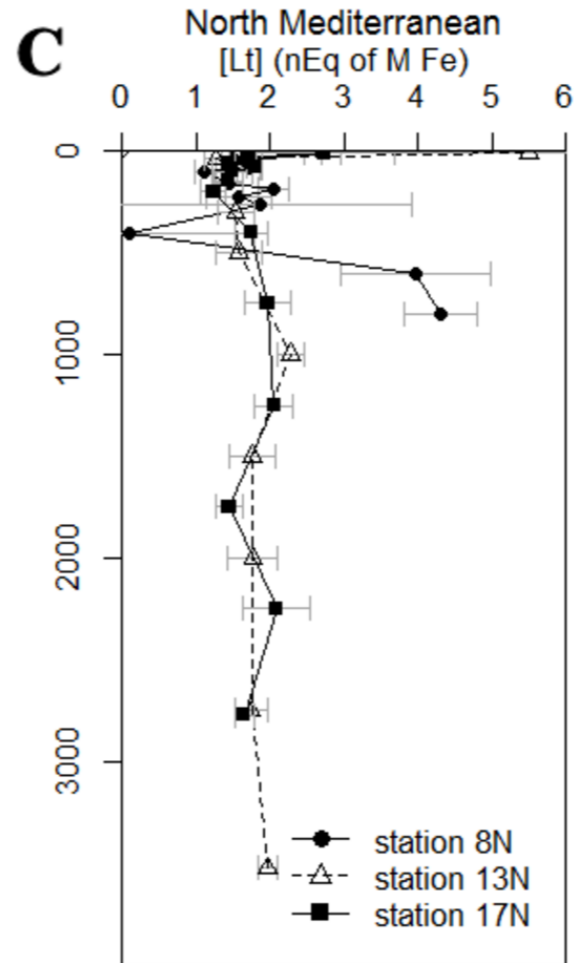
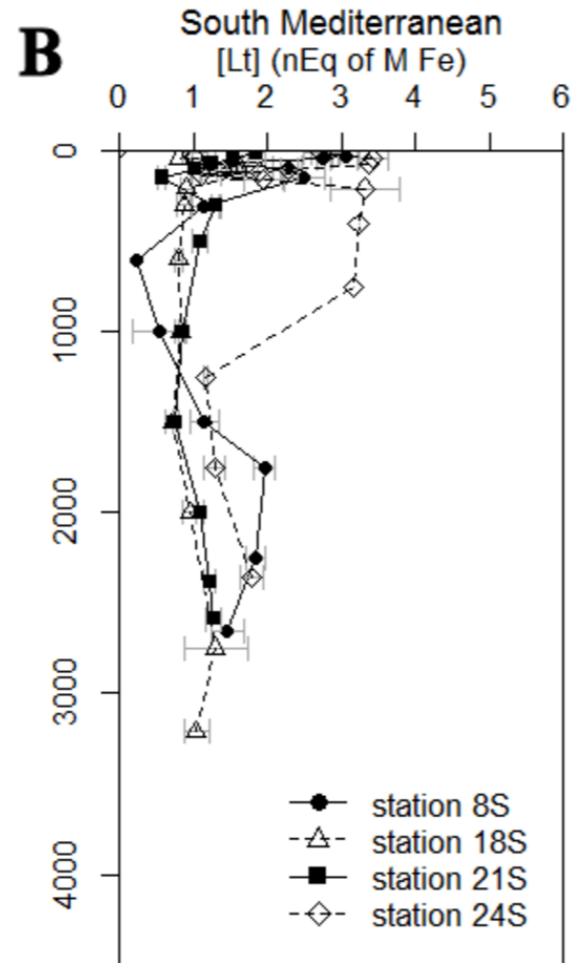
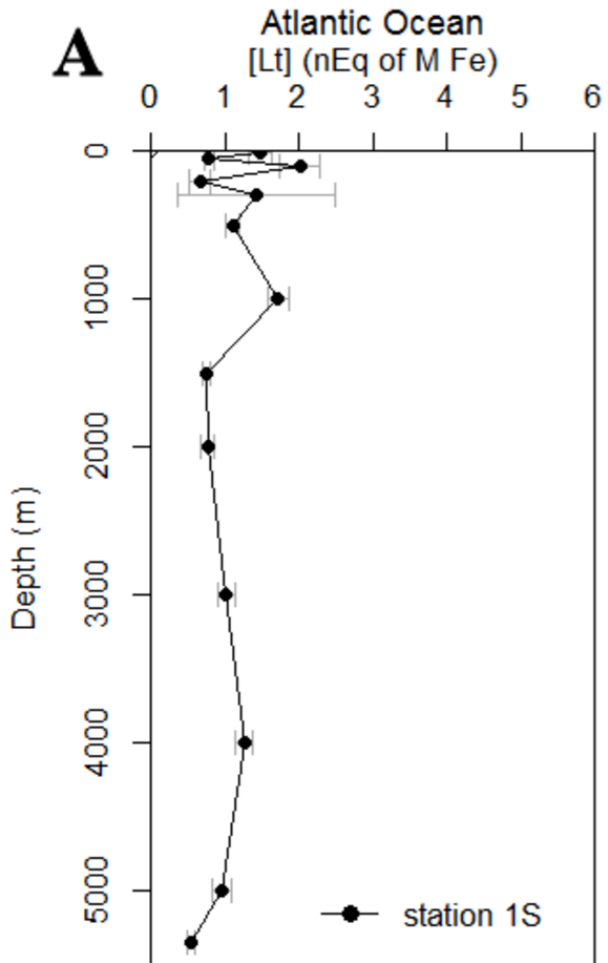












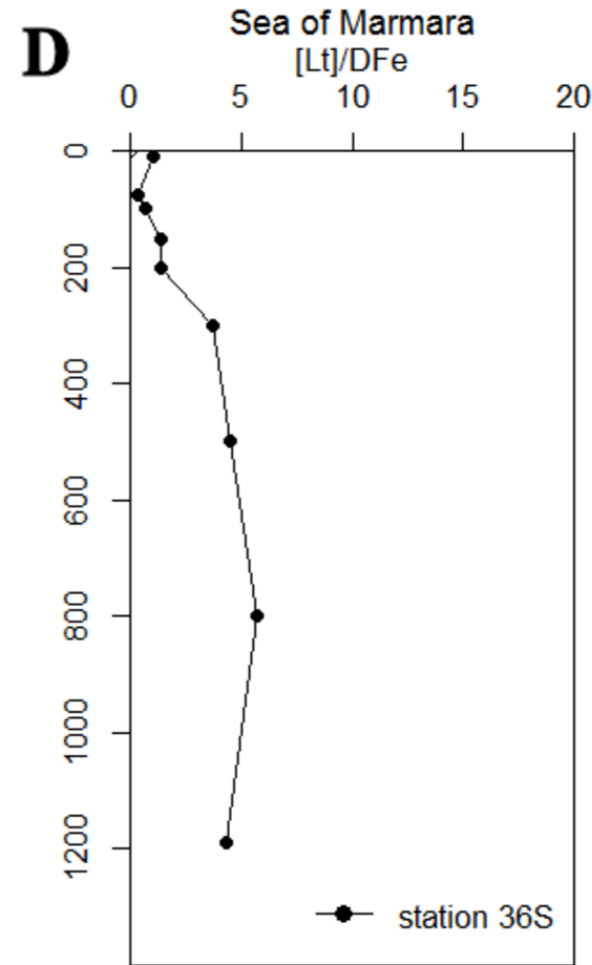
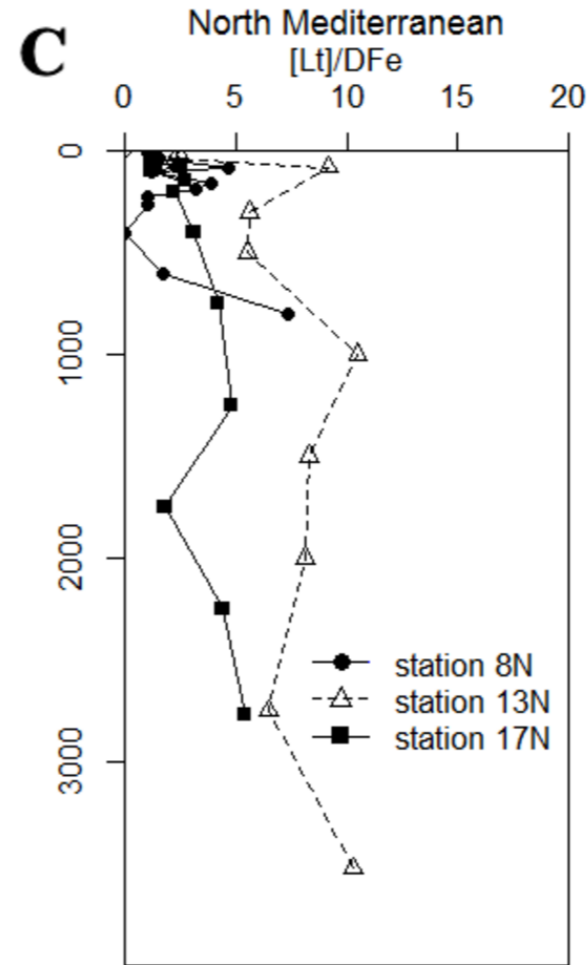
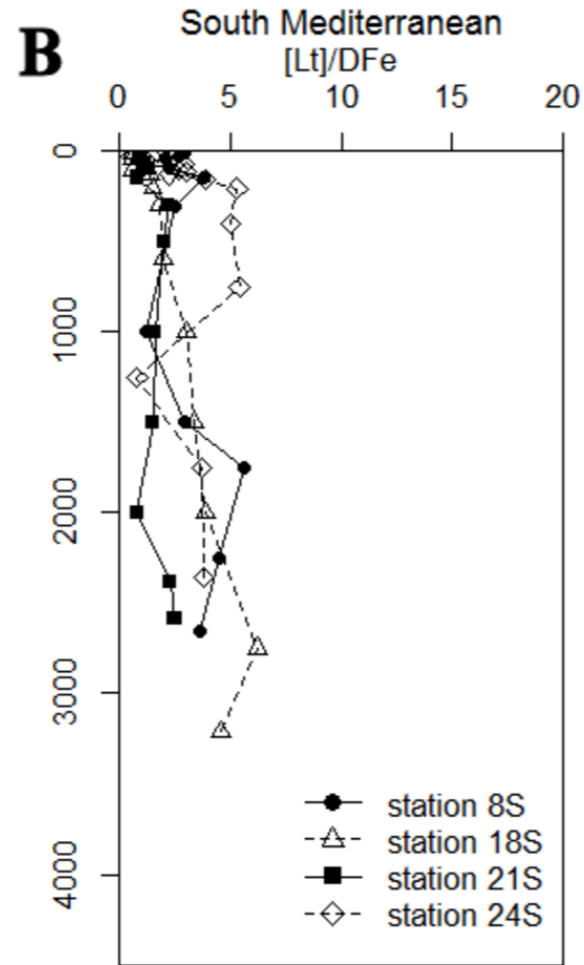
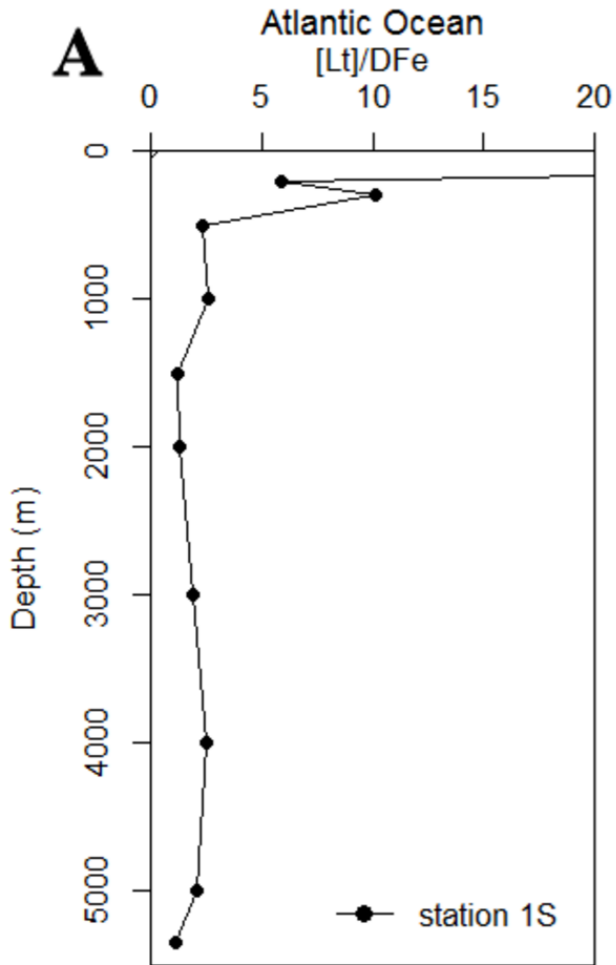


Table 1: Concentrations of SAFe and GEOTRACES reference samples in nM kg<sup>-1</sup>.

Columns show reference ID, the Intercalibration Consensus Values (ICV) and the bottle number of GS reference samples, the values measured during the cruises 64PE370 and 64PE374 in the North Atlantic Ocean, the Mediterranean Sea and the Sea of Marmara, including the standard deviation, and the number of sample analyses.

SAFe S is a surface, SAFe D is deep reference sample and GS is a GEOTRACES surface and GD is a GEOTRACES deep reference sample (<http://www.geotraces.org/science/intercalibration>).

<b>ID</b>	<b>ICV ± SE (nM kg<sup>-1</sup>)</b>	<b>Bottle nr</b>	<b>Measured ± SE (nM kg<sup>-1</sup>)</b>	<b>N</b>
<b>SAFe S</b>	0.093 ± 0.008	8,47,48,76	0.067 ± 0.013	7
<b>SAFe D2</b>	0.933 ± 0.023	29,191	0.963 ± 0.076	2
<b>GS</b>	0.546 ± 0.046	12	0.836 ± 0.030	3
		141	0.493 ± 0.021	2
		154	0.736 ± 0.007	2
		186	0.541	1
		55	0.473	1
<b>GD</b>	1.000 ± 0.100	87,238	1.088 ± 0.102	10

table 2A  
 median DFe with IQR and N

Region depth layer (m)	Atlantic Ocean			Mediterranean Sea			Western Basin			Eastern basin			Sea of Marmara		
	DFe nM	IQR	N	DFe nM	IQR	N	DFe nM	IQR	N	DFe nM	IQR	N	DFe nM	IQR	N
0-100	0.04	0.04	20	1.38	0.96	290	1.15	1.03	106	1.49	0.89	184	1.27	2.09	23
100-1000	0.38	0.42	38	0.54	0.37	472	0.57	0.41	170	0.53	0.33	302	0.52	0.28	21
1000-2000	0.67	0.07	15	0.37	0.31	120	0.40	0.19	49	0.34	0.42	71	0.47	0.76	4
>2000	0.56	0.08	21	0.35	0.24	118	0.39	0.25	47	0.34	0.25	71			

table 2B

depth layer m	N	logK' (M <sup>-1</sup> )	IQR	[Lt] (nEq of M Fe)	IQR	[L'] (nEq of M Fe)	IQR	[Lt]/DFe	IQR	Logalpha	IQR	[Fe'] (pM)	IQR
<b>Atlantic Ocean</b>													
0-100	2	22.06	0.44	1.13	0.35	1.10	0.35	43.4	20.5	13.07	0.29	0.03	0.01
100-1000	4	21.71	0.44	1.27	0.58	0.95	0.86	8.0	13.7	12.73	0.53	0.52	0.54
1000-2000	3	22.04	0.34	0.77	0.49	0.19	0.48	1.3	0.7	12.37	0.16	3.44	0.80
>2000	4	21.88	0.23	0.99	0.23	0.50	0.19	2.0	0.5	12.52	0.19	1.87	0.63
<b>whole Mediterranean</b>													
0-100	48	21.93	0.67	1.70	1.00	0.45	1.08	1.4	1.2	12.50	1.00	3.28	26.11
100-1000	61	21.78	0.58	1.30	0.82	0.67	0.97	2.2	1.6	12.61	0.57	1.64	2.39
1000-2000	14	21.89	0.54	1.32	0.58	0.83	0.86	3.3	2.5	12.69	0.44	0.84	1.10
>2000	13	21.57	0.26	1.45	0.57	1.09	0.68	4.4	2.9	12.67	0.34	0.92	0.55
<b>East Mediterranean</b>													
0-100	24	21.94	0.64	1.74	1.36	0.57	1.20	1.4	1.2	12.72	0.98	1.77	14.83
100-1000	24	21.66	0.52	1.51	0.82	0.89	0.84	2.7	2.0	12.49	0.23	1.99	1.27
1000-2000	8	21.55	0.41	1.61	0.43	1.24	0.70	4.0	3.4	12.54	0.41	0.92	0.84
>2000	8	21.57	0.18	1.70	0.68	1.39	0.70	4.5	2.7	12.71	0.68	1.11	11.55
<b>West Mediterranean</b>													
0-100	22	21.87	0.49	1.64	0.66	0.24	0.72	1.2	0.9	12.36	1.12	5.25	48.79
100-1000	39	21.87	0.64	1.21	0.80	0.55	0.83	2.0	1.7	12.72	0.63	1.42	3.09
1000-2000	6	22.13	0.27	1.02	0.35	0.37	0.59	2.5	2.7	12.84	1.60	0.68	173.00
>2000	5	21.57	0.46	1.27	0.08	0.82	0.33	3.8	2.1	12.67	0.40	0.92	0.42
<b>Sea of Marmara</b>													
0-100	3	21.56	0.44	2.93	2.12	0.01	0.11	0.7	0.4	10.50	1.30	1160.0	1074.8
100-1000	5	21.20	0.31	1.81	0.81	1.33	1.12	3.7	3.1	11.82	0.86	9.24	17.72
>1000	1	21.82		0.79		0.61		4.3		12.61		0.57	